# A bacterial effector counteracts host autophagy by promoting degradation of an autophagy component

Jia Xuan Leong[1], Margot Raffeiner[2], Daniela Spinti[2], Gautier Langin[1], Mirita Franz-Wachtel[3], Andrew R. Guzman[4], Jung-Gun Kim[4], Pooja Pandey[5], Alyona E. Minina[6], Boris Macek[3], Anders Hafrén[8], Tolga O. Bozkurt[5], Mary Beth Mudgett[4], Frederik Börnke[2,7], Daniel Hofius[8], Suayib Üstün[1*]

[1]University of Tübingen, Center for Plant Molecular Biology (ZMBP), 72076 Tübingen, Germany
[2]Leibniz-Institute of Vegetable and Ornamental Crops (IGZ), 14979 Großbeeren, Germany
[3]Interfaculty Institute for Cell Biology, Department of Quantitative Proteomics, University of Tübingen, 72076 Tübingen, Germany.
[4]Department of Biology, Stanford University, Stanford, CA 94305, USA
[5]Department of Life Sciences, Imperial College London, SW7 2AZ London, United Kingdom.
[6]Department of Molecular Sciences, Uppsala BioCenter, Swedish University of Agricultural Sciences and Linnean Center for Plant Biology, 75007 Uppsala, Sweden.
[7]Institute of Biochemistry and Biology, University of Potsdam, 14476 Potsdam, Germany
[8]Department of Plant Biology, Uppsala BioCenter, Swedish University of Agricultural Sciences and Linnean Center for Plant Biology, 75007 Uppsala, Sweden.

**Keywords:** Autophagy, Effectors, Immunity, Ubiquitination, Disease, Xenophagy

*Corresponding author
suayib.uestuen@zmbp.uni-tuebingen.de

**Abstract:**
Beyond its role in cellular homeostasis, autophagy plays anti- and pro-microbial roles in host-microbe interactions, both in animals and plants. One prominent role of anti-microbial autophagy is to degrade intracellular pathogens or microbial molecules, in a process termed xenophagy. Consequently, microbes evolved mechanisms to hijack or modulate autophagy to escape elimination. Although well-described in animals, the extent to which xenophagy contributes to plant-bacteria interactions remains unknown. Here, we provide evidence that *Xanthomonas campestris* pv. *vesicatoria (Xcv)* suppresses host autophagy by utilizing type-III effector XopL. XopL interacts with and degrades the autophagy component SH3P2 via its E3 ligase activity to promote infection. Intriguingly, XopL is targeted for degradation by defense-related selective autophagy mediated by NBR1/Joka2, revealing a complex antagonistic interplay between XopL and the host autophagy machinery. Our results implicate plant antimicrobial autophagy in depletion of a bacterial virulence factor and unravels an unprecedented pathogen strategy to counteract defense-related autophagy.

## Introduction

Eukaryotic cells react dynamically to external and internal stimuli by adjusting their proteome. This requires a stringent regulation of protein homeostasis which is achieved in large part by regulated protein degradation. Cellular degradation machineries including the proteasome and autophagy maintain protein homeostasis by recycling unwanted or dysfunctional proteins (Pohl & Dikic, 2019). While the proteasome degrades short-lived proteins or mis-folded proteins, autophagy can remove larger protein complexes, insoluble aggregates, entire organelles as well as pathogens. Under normal conditions, both degradation pathways are critical for cellular housekeeping functions, while under stress conditions they facilitate the reorganization of the proteome to adapt to a changing environment (Marshall & Vierstra, 2018).

Regulated proteolytic degradation by proteasome has been identified as an essential component of immunity influencing the outcome of host-microbe interactions across kingdoms (Adams & Spoel, 2018; Hu & Sun, 2016). In the recent years, autophagy has also emerged as a central player in immunity and disease in humans and plants (Germic *et al*, 2019; Leary *et al*, 2019; Levine *et al*, 2011; Üstün *et al*, 2017; Yang & Klionsky, 2020). In mammals, autophagy has various connections to several diseases, regulating cell death and innate immunity (Germic *et al*, 2019; Yang & Klionsky, 2020). Dual roles have also been ascribed to autophagy in host-bacteria interactions (Mostowy, 2013). While some bacterial pathogens recruit the autophagy machinery in order to create a replicative niche (pro-bacterial autophagy), anti-bacterial autophagy removes bacterial intruders to limit pathogen infection (Huang & Brumell, 2014). The elimination of bacteria is a selective autophagy response, termed xenophagy (Gomes & Dikic, 2014). In this process, bacterial pathogens such as *Salmonella* and *Shigella* are degraded by autophagy through a ubiquitin-dependent mechanism (Dupont *et al*, 2009; van Wijk *et al*, 2012). This demonstrates that autophagy is not only a largely unspecific ("bulk") catabolic and recycling process, as increasing evidence now indicates that autophagy also acts as a selective mechanism to degrade protein aggregates, organelles and pathogens. Selectivity is mediated by autophagy receptors, of which p62 and NBR1 play key roles in controlling pathogenic infection in mammals (Gomes & Dikic, 2014). Both autophagy receptors can bind to ubiquitinated bacteria, and degrade them, through their ability to bind autophagosome-associated ATG8 proteins (Gomes & Dikic, 2014).

It is known that type-III effector (T3E) proteins of plant pathogenic bacteria are present in the host cell while bacteria reside in the extracellular space. These effectors are able to manipulate host defense responses for the benefit of the pathogen (Khan *et al*, 2018). Very recently, it has been shown that microbial effectors perturb or hijack degradation machineries to attenuate plant immune reactions (Banfield, 2015; Langin *et al*, 2020). For instance, *Pst* activates autophagy via the action of the T3E HopM1 to degrade the proteasome and suppress its function in a

process termed proteaphagy (Üstün *et al*, 2018; Üstün *et al*, 2016). Although this process can be categorized as a pro-bacterial role of autophagy, NBR1-mediated anti-bacterial autophagy seems to restrict lesion formation and pathogenicity of *Pst* (Üstün & Hofius, 2018). The dual role of autophagy in plant-bacteria interactions is further confirmed by findings that certain effectors are also able to suppress autophagy responses, although the understanding of the exact molecular mechanisms are still very limited (Lal *et al*, 2020). In addition, plant NBR1, which is also referred as Joka2 in solanaceous species, is able to restrict growth and disease progression of the plant pathogenic oomycete *Phytophthora infestans* (Dagdas et al, 2016; Dagdas et al, 2018). Recently, plant NBR1-mediated xenophagy was described to remove intracellular viral proteins (Hafrén *et al*, 2017; Hafrén *et al*, 2018). These studies demonstrated that, similar to that in mammals, plant NBR1 participates in xenophagy by degrading viral proteins. Given the fact that plant pathogenic bacteria reside in the extracellular space and the presence of T3Es inside the host cell it is not known whether NBR1-mediated xenophagy might play a role in plant-microbe interactions by targeting intracellular T3Es.

Like *Pst*, *Xanthomonas campestris* pv. *vesicatoria (Xcv)* is another well-studied hemi-biotrophic bacterium, causing disease on tomato and pepper plants (Timilsina *et al*, 2020). Mounting evidence has been established that *Xcv* and its T3Es exploit plant ubiquitin- and ubiquitin-like pathways (Buttner, 2016; Üstün & Börnke, 2014). While the role of the proteasome system in *Xanthomonas* infections is well understood, little is known about how autophagy shapes the outcome of *Xanthomonas*-host interactions. Recent findings in the cassava- *Xanthomonas axonopodis* pv. *manihotis* (*Xam*) model suggest that autophagy has an anti-bacterial role (Yan et al, 2017; Zeng et al, 2018). However, our current understanding about how T3Es might modulate and regulate this response is very limited. Are there similar mechanisms operating in pro- and antibacterial roles across different pathogenic bacteria? Do plants utilize xenophagy as an anti-bacterial mechanism to degrade pathogenic components in plant-bacteria interactions?

To address these questions, we performed a mechanistic analysis of the interplay of plant defence-related autophagy and *Xcv* pathogenesis. Here, we provide evidence that NBR1/Joka2 degrades T3E XopL, which in turn is used by *Xcv* to block autophagy via its E3 ligase activity by degrading autophagy component SH3P2 in a proteasome-dependent manner. This prevents T3E XopL from being targeted for degradation by the selective autophagy receptor NBR1/Joka2. We show that specificity in autophagy pathways play a role during plant-pathogen interactions.

## Results

***Xanthomonas blocks autophagy in an effector-dependent manner to promote pathogenicity***

Given the prominent role of autophagy in host-microbe interactions, we investigated autophagic response after *Xanthomonas* infection. To this end we used the model plant *Nicotiana benthamiana*, since methods such as Agrobacterium-mediated transient expression, virus-induced gene silencing (VIGS), and autophagy activity reporter assays are well-established and reproducible. Assays were conducted with a *Xcv* strain harboring a deletion in the T3E XopQ (*Xcv ΔxopQ)*, which is a host range determinant in *Nicotiana* species (Adlung *et al*, 2016), thus restoring the full virulence of *Xcv* in *Nicotiana benthamiana* in the absence of XopQ.

First, we monitored autophagosome formation using RFP-ATG8g which is a structural component of autophagosomes and is widely used to label these structures (19). We infected *N. benthamiana* plants transiently expressing RFP-ATG8g with *Xcv ΔxopQ* and monitored autophagosomal structures during Concanamycin A (ConA) treatment. ConA is an inhibitor of vacuolar acidification that blocks autophagic body degradation (Minina *et al*, 2018; Svenning *et al*, 2011). In the absence of ConA, *Xcv ΔxopQ* induced massive accumulation of autophagosome-like structures which could not be further enhanced by the presence of ConA

(Fig. 1A). This suggests that *Xcv* blocks autophagic degradation *in planta*. To provide additional evidence that these structures are indeed autophagosomes, we imaged *N. benthamiana* plants which were silenced using VIGS for *ATG7*, a crucial component of the autophagy pathway, and transiently expressing GFP-ATG8e, and found that the structures that accumulated under Xcv infection after 6hpi or AZD8055 treatment, a compound known to induce autophagy, no longer accumulating (Fig. S1A). The induction of autophagosome formation and suppression of autophagic degradation prompted us to investigate host autophagy by immunoblotting for endogenous ATG8 and Joka2 in *N. benthamiana* (Dagdas *et al*, 2016; Svenning *et al*, 2011). We also used the previously described autophagy suppressor AIMp, a small peptide sequence derived from the *Phytophthora* PexRD54 effector (Pandey *et al*, 2021), as a positive control for autophagy suppression. Joka2 protein abundance increased during infection, to a small extent 1-day post-inoculation (dpi), and to a greater extent at 2 dpi, while ATG8 protein levels only slightly increased at 2 dpi (Fig. 1B). Protein accumulation seen during immunoblotting could be attributed to increased transcription and/or decreased degradation. Thus, to uncouple these effects we utilized a quantitative autophagy assay to measure autophagic degradation during infection. This assay is based on Agrobacterium-mediated transient expression of 35S promoter-driven *Renilla* luciferase (RLUC) fused to ATG8a (RLUC-ATG8a) or NBR1 (RLUC-NBR1), together with free *Firefly* luciferase (FLUC) which serves as an internal control for expression as it is not degraded with autophagy (Dauphinee *et al*, 2019; Üstün *et al.*, 2018). The autophagy reporter assay revealed that *Xcv ΔxopQ* infection led to a significant increase of RLUC-ATG8a/FLUC and RLUC-NBR1/FLUC ratios, suggesting reduced autophagic turnover after 2dpi (Fig. 1C, Fig. S1B). Another indicator of impaired autophagy is the increased gene expression of the autophagic markers (Minina *et al*, 2018). Transcript levels of *Joka2*, *NbATG8-2.1/2* and *NbATG8-1.1/1.2* were significantly higher compared to mock infection at 2 dpi (Fig. 1D), with *NbATG8-2.1/2.2* showing an earlier increase than the two other genes and suggesting at a differential response of NbATG8 isoforms during *Xcv* infection. Taken together with previous results, accumulation of Joka2 protein levels at 1 dpi which was observed earlier than its induced gene expression at 2 dpi, as well as reduced autophagic turnover after 6 hpi using the autophagy reporter assay (Fig. S1B) strongly suggest that *Xcv* dampens autophagic flux. To assess the biological relevance of suppressed autophagic degradation during *Xcv* infection, we determined bacterial growth in *N. benthamiana roq1* plants which carry a mutation in *Recognition of XopQ 1 (Roq1)* that recognizes the effector XopQ to activate resistance to *Xcv* (Gantner *et al*, 2019; Schultink *et al*, 2017). In these plants we transiently expressed RFP-AIMp as an autophagy suppressor. At 6 dpi, *Xcv* growth was significantly elevated in *roq1* plants transiently expressing RFP-AIMp compared to empty vector (EV) control (Fig. 1E). The same trend was observed when *ATG7* was silenced using VIGS in *N. benthamiana,* as *ATG7* silencing rendered plants more susceptible to *Xcv* Δ*xopQ* at 6 dpi (Fig. S2).

Because T3Es were previously shown to modulate proteasome function and autophagy (Üstün et al, 2018; Üstün et al, 2016; Üstün *et al*, 2013), we analyzed host autophagy response to a nonpathogenic type-III secretion system (T3SS) mutant *Xcv ΔhrcN*, which is unable to drive secretion of T3Es (Lorenz & Buttner, 2009). In contrast to *Xcv ΔxopQ*, the T3SS-deficient mutant *Xcv ΔhrcN* did not alter the protein abundance of ATG8 and Joka2 (Fig. S3A), nor RLUC-ATG8a/FLUC or RLUC-NBR1/FLUC ratio (Fig. S3B) or transcript abundance of autophagy marker genes *NbJoka2* and *NbATG8-1.1/1.2* (Fig S3C). Together, these data support the model that *Xcv* blocks autophagy in a T3E-dependent manner to promote virulence.

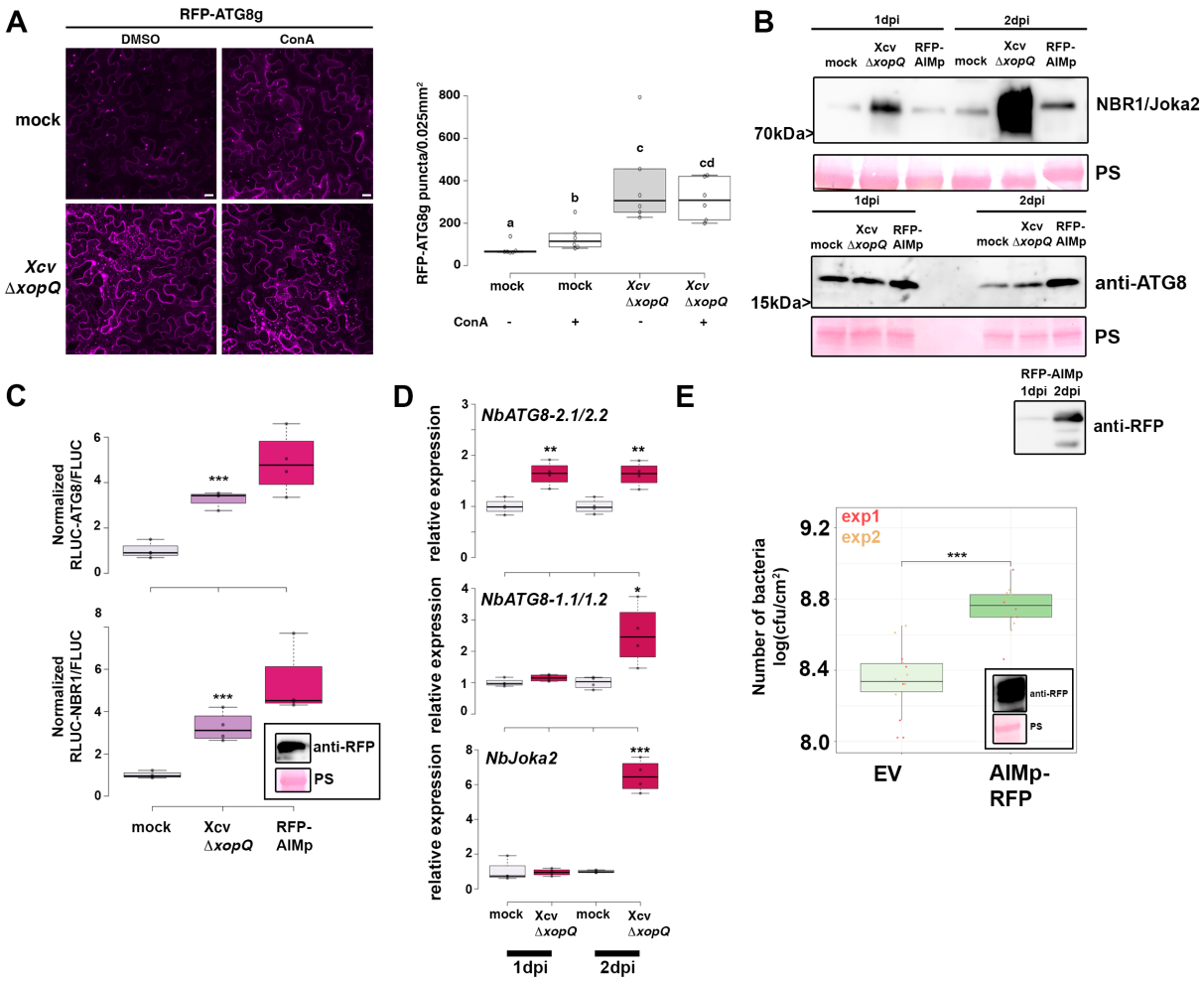


**Figure 1: Xanthomonas blocks autophagy to enhance its pathogenicity**

**(A)** RFP-ATG8g-labeled autophagosomes were quantified from plants infected with mock or Xcv *ΔxopQ* at 2 dpi in the presence or absence of ConA (bars = 20 µm). Puncta were calculated from z-stacks (15) of *n*=6 individuals using ImageJ. Data points are plotted as open circles. Different letters indicate statistically different groups ($P < 0.05$) as determined by one-way ANOVA. The experiment was repeated twice with similar results.

**(B)** Immunoblot analysis of NBR1 and ATG8 protein levels in Xcv *ΔxopQ* or mock infected *N. benthamiana* plants at 1 and 2dpi. Agrobacterium-mediated transient expression of AIMp-RFP serves as a control for autophagy suppression. Ponceau Staining (PS) served as a loading control. The experiment was repeated three times with similar results.

**(C)** RLUC-ATG8a or RLUC-NBR1 constructs were coexpressed with internal control FLUC in *N. benthamiana*. *Xcv ΔxopQ* was co-infiltrated with Agrobacteria containing the luciferase reporter constructs. Coexpression of RFP-AIMp serves as a control for autophagy inhibition. Expression of the latter was confirmed with western blot (inset). *Renilla* (RLUC) and *Firefly* (FLUC) luciferase activities were simultaneously measured in leaf extracts at 48 h post-infiltration using the dual-luciferase system (n=4). Statistical significance (***$P<0.001$) was revealed by Student's *t*-test. The experiment was repeated more than 3 times with similar results.

**(D)** RT-qPCR analysis of *NbATG8-1.1/1.2, NbATG8-2.1/2.2* and *NbJoka2* transcript levels upon challenge of *N. benthamiana* plants with Xcv *ΔxopQ* for 1 and 2 dpi compared to mock infected plants. Values represent expression relative to mock control of respective time point

198 and were normalized to *Actin*. Statistical significance (**P* < 0.05, ***P* < 0.01, *** *P* < 0.001)
199 was revealed by Student's *t*-test.
200 **(E)** Bacterial density in leaves of *N. benthamiana roq1* infected with *Xcv* in the presence or
201 absence autophagy suppressor AIMp-RFP. Leaves were syringe-infiltrated with $OD_{600}$ =
202 0.0004, and colony-forming units were counted at 6 dpi. Compared to empty vector control
203 (EV), AIMp expressing plants (n=6) harbour significantly more bacteria. Bacterial growth was
204 repeated with the same result in 12 plants over two independent experiments. Red and yellow
205 data points indicate independent repeats of the experiment. Statistical significance (****P* <
206 0.001) was revealed by Student's *t*-test. Expression of RFP-AIMp was verified at 6 dpi with an
207 anti-RFP blot (inset).
208
209 ***T3E XopL suppresses autophagy***
210 To address which T3E(s) might manipulate autophagy, we screened for *Xcv* effectors XopJ,
211 XopD and XopL which have known function in modulating proteolytic degradation pathways
212 (Üstün & Börnke, 2014; Kim *et al*, 2013; Singer *et al*, 2013; Üstün *et al*, 2015; Üstün & Börnke,
213 2015) as well as XopS which has not been described to modulate degradation machineries. To
214 this end, we used the quantitative dual-luciferase autophagy reporter assay. Transient
215 expression of XopL, a previously characterized E3 ligase (Singer *et al*, 2013), and XopJ, an
216 effector previously shown to inhibit host proteasome, led to a significant increase in RLUC-
217 ATG8a/FLUC and RLUC-NBR1/FLUC ratio (Fig. 2A, S4A), which was consistent across
218 multiple experiments. In contrast, transient expression of XopD and XopS had no evident effect
219 on autophagic degradation (Fig. S4A). We chose to study XopL further, as XopJ was previously
220 shown to inhibit host proteasome (Üstün *et al*, 2013), which may result in modulation of
221 autophagy as shown by the effect of treatment with a proteasome inhibitor MG132 (Fig. S4B).
222 Performing immunoblot analysis of ATG8 protein levels in *N. benthamiana* leaves, we found
223 that transient expression of XopL resulted in an accumulation of NBR1 and ATG8 proteins at
224 2 dpi (Fig. 2B). While this was also consistent with elevated gene expression of ATG8,
225 NBR1/Joka2 expression was only induced at 1 dpi but not 2 dpi upon XopL expression (Fig.
226 S4C). Transient expression of the autophagy inhibitor AIMp showed similar expression trends
227 (Fig. S4C). Treatment with ConA revealed that ATG8 levels could not be further enhanced
228 when XopL was expressed (Fig. 2C), providing strong evidence that XopL inhibits autophagic
229 turnover. We note that XopL accumulates under ConA treatment (Fig. 2C), which suggests that
230 XopL is also subject to autophagic degradation.
231 To validate that XopL also acts as an autophagy suppressor during *Xcv* infection we constructed
232 a *xopL* deletion mutant in *Xcv* WT and *Xcv ΔxopQ* backgrounds. *Xcv ΔxopL* displayed reduced
233 growth and symptom development upon infection of tomato plants and the same, but to a lesser
234 extent, was observed for *Xcv ΔxopL* in *N. benthamiana* (Fig S5A-E), demonstrating that XopL
235 has a role during infection. Monitoring autophagosome-like structures in leaves transiently
236 expressing GFP-ATG8e revealed that tissue infected with *Xcv ΔxopL* induced fewer GFP-
237 ATG8e puncta than *Xcv* in the absence of ConA (Fig 2D, Fig S6A). Addition of ConA increased
238 GFP-ATG8e puncta in leaves infected with *Xcv ΔxopL* but not in *Xcv*, indicating that XopL has
239 a role in dampening autophagy during infection (Fig. 2D). By analyzing ATG8 and NBR1
240 protein levels, we also verified that XopL partially contributes to ATG8 and NBR1/Joka2
241 accumulation (Fig. 2E), supporting the notion that XopL suppresses autophagic degradation.
242 We confirmed this when we monitored RFP-Joka2 in transiently expressing *N. benthamiana*
243 *roq1* plants after Xcv infection. Infection with *Xcv* resulted in an induction of NBR1/Joka2
244 bodies in comparison to *Xcv ΔxopL* infected leaves (Fig. S6B). Utilizing the quantitative dual-
245 luciferase autophagy assay, we show that *Xcv ΔxopQ ΔxopL* was unable to suppress autophagy
246 to levels observed in tissues infected with *Xcv ΔxopQ* levels, both at 2dpi (Fig. 2F), indicating
247 that XopL has a major impact on autophagy during infection. However, *Xcv ΔxopQ ΔxopL* still

leads to a slight increase in both RLUC-ATG8a/FLUC and RLUC-NBR1/FLUC ratios, suggesting that *Xcv* possesses another T3E with a redundant function.

To analyze whether XopL has similar functions in other plant species, we generated transgenic *Arabidopsis thaliana* lines expressing GFP-XopL under the UBQ10 promoter. Similar to the results we obtained in *N. benthamiana*, GFP-XopL transgenic *A. thaliana* plants showed increased NBR1 protein abundance in the absence and presence of ConA treatment (Fig. S7A), suggesting a block of NBR1 turnover. The early senescence phenotype of transgenic lines expressing XopL (Fig. S7B) and elevated gene expression of *ATG8a* and *NBR1* is indicative of altered autophagy activity (Fig. S7D). Imaging with confocal microscopy revealed that GFP-XopL localizes to punctate structures in *A. thaliana* leaf epidermal cells (Fig. S7C).

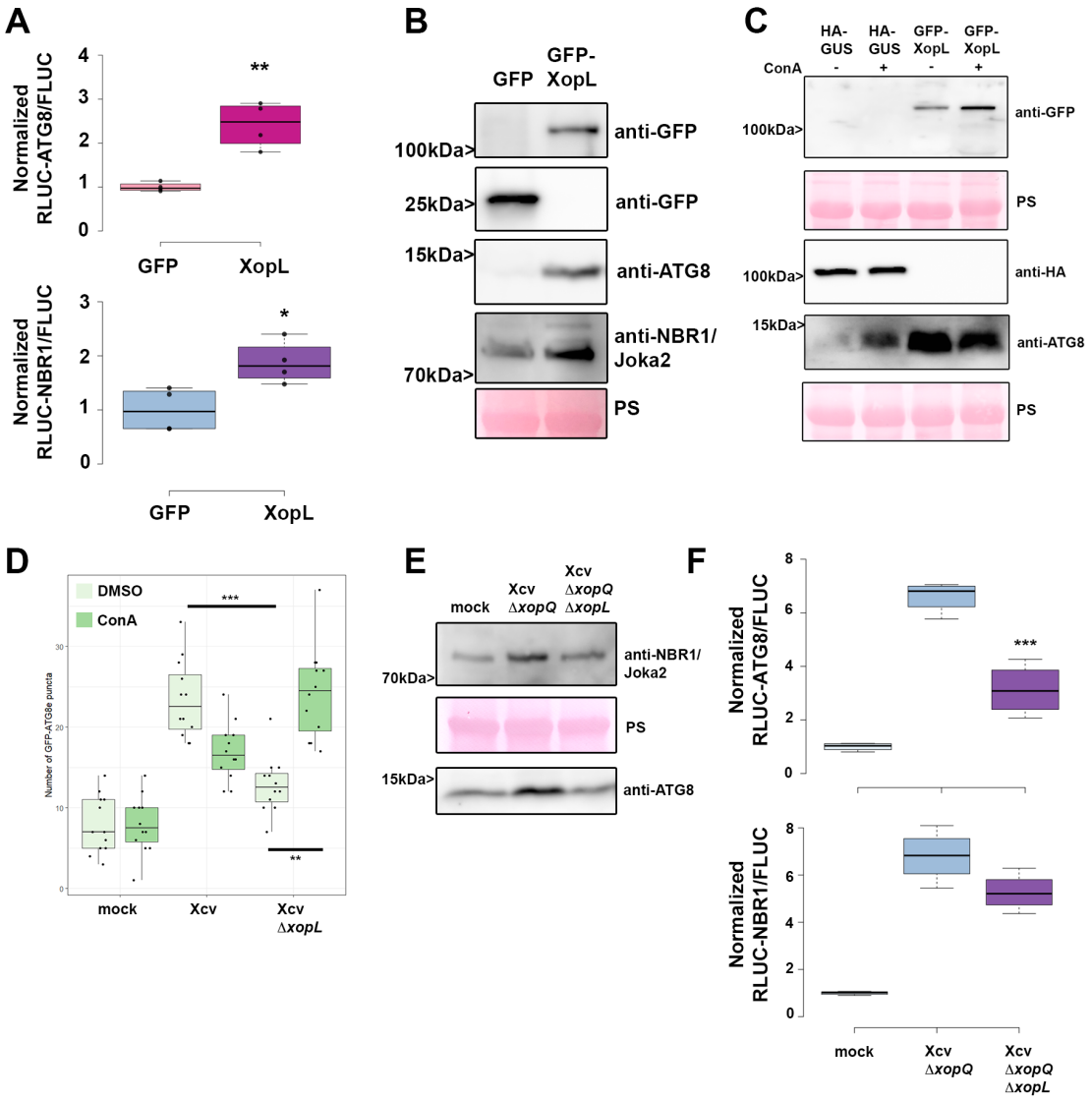


**Figure 2: Xanthomonas T3E XopL is suppressing autophagy**

**(A)** RLUC-ATG8a or RLUC-NBR1 constructs were coexpressed with internal control FLUC in *N. benthamiana*. XopL or GFP constructs were co-infiltrated. RLUC and FLUC signals were simultaneously measured in leaf extracts at 48 h post- infiltration using the dual-luciferase system. Values represent the ratio of RLUC-ATG8a and FLUC activities to the mean of control (n=4). Statistical significance ($P < 0.01$) was shown by Student's *t*-test. The experiment was repeated more than 3 times by with similar results.

**(B)** Immunoblot analysis of NBR1 and ATG8 protein levels in *N. benthamiana* plants transiently expressing GFP-XopL or GFP control at 2dpi verified with an anti-GFP antibody. Ponceau Staining (PS) served as a loading control. The experiment was repeated at least three times with similar results.
**(C)** Immunoblot analysis of NBR1 and ATG8 protein levels in *N. benthamiana* plants transiently expressing XopL or GUS control at 2dpi after ConA or DMSO treatment. Expression of GFP-XopL was verified with an anti-GFP antibody, while expression of GUS-HA was confirmed with an anti-HA antibody. Ponceau Staining (PS) served as a loading control. The experiment was repeated twice with similar results.
**(D)** GFP-ATG8g-labeled autophagosomes were quantified from plants infected with *Xcv ΔxopQ* or *Xcv ΔxopQ ΔxopL* at 2 dpi in the presence or absence of ConA. Puncta were calculated from z-stacks (15) of $n$=12 individuals using ImageJ. Statistical significance (** $P < 0.01$, *** $P < 0.001$) was determined by one way ANOVA. The experiment was repeated twice with similar results.
**(E)** Immunoblot analysis of NBR1 and ATG8 protein levels in Xcv *ΔxopQ,* Xcv *ΔxopQ ΔxopL* or mock infected *N. benthamiana* plants at 2dpi. Ponceau Staining (PS) served as a loading control. The experiment was repeated twice with similar results.
**(F)** RLUC-ATG8a or RLUC-NBR1 constructs were coexpressed with internal control FLUC in *N. benthamiana*. *Xcv ΔxopQ and Xcv ΔxopQ ΔxopL* were co-infiltrated with Agrobacteria containing the respective constructs. RLUC and FLUC activities were simultaneously measured in leaf extracts at 48 h post- infiltration using the dual-luciferase system. Statistical significance comparing *Xcv ΔxopQ and Xcv ΔxopQ ΔxopL* values (***$P < 0.001$) was revealed by Student's $t$-test. The experiment was repeated 3 times with similar results.

***XopL interacts with and degrades the autophagy component SH3P2 contributing to Xcv virulence during infection***

Previously, XopL was characterized as belonging to a novel class of E3 ligases and is capable of suppressing plant defense responses. There are no known plant targets of XopL (Singer *et al*, 2013), so we carried out a yeast-two hybrid (Y2H) screen using a cDNA library from tobacco (*Nicotiana tabacum*) to investigate whether XopL directly targets autophagy components to act as an autophagy suppressor. Our previous interactions studies indicate that the tobacco cDNA library is sufficient to identify host targets of *Xcv* T3Es that are conserved across different plant species, such as pepper, tomato and *A. thaliana* (Albers *et al*, 2019; Üstün *et al.*, 2013; Üstün *et al*, 2014). One cDNA identified in the Y2H screening for XopL interacting proteins encoded a homologue of *A. thaliana* SH3P2, which has an amino acid identity of 74 % to the *N. tabacum* homologue (Fig S8A). Homologues are also present in *Nicotiana benthamiana* (NbSH3P2a and NbSH3P2b, 98% identity) and tomato (SlSH3P2, 96% to NtSH3P2) (Fig S8A, B). Direct interaction assays in yeast revealed that XopL is able to interact with SH3P2 from *N. tabacum* and *N. benthamiana* (Fig. 3A and Fig. S8C). SH3P2 from *A. thaliana* was previously identified as a novel autophagy component that interacts with ATG8 and binds to phosphatidylinositol 3-phosphate (PI3P) to regulate autophagosome formation, having also a potential role in late events of autophagosome biogenesis (Zhuang & Jiang, 2014; Zhuang *et al*, 2013). SH3P2 was also found to play a role in the recognition of ubiquitinated membrane proteins, and in targeting them to the endosomal sorting complexes required for transport (ESCRT) machinery (Nagel *et al*, 2017). We next sought to determine whether the interaction between XopL and SH3P2 occurs *in planta*. Due to expression problems of tobacco SH3P2 and also due to their high identity, we conducted further interaction studies with AtSH3P2. Using bimolecular fluorescence complementation (BiFC) and in *vivo* co-immunoprecipitation (co-IP), we found that XopL and AtSH3P2 interact in the plant cell, in small punctate structures resembling autophagosomes and also in larger structures (Fig. 3B and C; Supp Video 1). Additional *in vitro* co-IP data, using *E. coli* produced recombinant MBP-XopL and GST-*At*SH3P2, suggests that

XopL and SH3P2 might directly interact with each other (Fig. S8D). Given the fact that SH3P2 from *A. thaliana* interacts with ATG8 and XopL localizes in puncta within plant cells (Zhuang *et al*, 2013; Erickson *et al*, 2018), we assessed whether XopL co-localizes with autophagosomes *in planta*. We were able to identify that transient expression of GFP-XopL in *N. benthamiana* with the autophagosome markers RFP-ATG8e and SH3P2-RFP resulted in co-localization (Fig. 3D). SH3P2 also co-localized with ATG8e upon transient co-expression in *N. benthamiana* (Fig. Fig.3D). This further supports the idea that XopL is functioning in the autophagy pathway by associating with these components *in planta*. Since XopL possesses E3 ligase activity, we next sought to investigate whether XopL might destabilize SH3P2 via ubiquitination, and thereby block autophagic degradation. Indeed, *in planta* transient co-expression of GFP-XopL and AtSH3P2-GFP resulted in a reduction in the latter's protein abundance in *N. benthamiana* (Fig. 3E).

Previously, downregulation of SH3P2 in *A. thaliana* has been shown to reduce autophagic activity (Zhuang *et al*, 2013). However, the role of SH3P2 is still controversial, as another study identified that SH3P2 functions in clathrin-mediated endocytosis without having any obvious effects on dark-induced autophagy (Nagel *et al*, 2017). To shed light on the enigmatic and versatile function of SH3P2, we used VIGS in *N. benthamiana* targeting both endogenous isoforms *NbSH3P2a* and *b*. Silencing had no obvious phenotypic effect on plants, and silencing efficiency was assessed by qPCR (Fig. S9A and B). Subsequent immunoblot analysis revealed that in comparison to the pTRV2-GFP control, SH3P2 VIGS plants displayed accumulation of ATG8 protein levels, similar results to that reported by Zhuang et al. 2013 (Fig. S9C). To corroborate this finding, we transiently expressed GFP-ATG8e in control and silenced plants and monitored autophagosome formation upon AZD8055 treatment, a TOR inhibitor and autophagy activator. The number of autophagosomes increased upon AZD8055 treatment in both plants but were significantly less in SH3P2 VIGS plants when treated with ConA (Fig. S9D). This indicates that downregulation of SH3P2 in *N. benthamiana* impairs maturation of autophagosomes and hence autophagic degradation. Indeed, using confocal microscopy and GFP-ATG8e labelling, we observed aberrant autophagosomal structures in VIGS SH3P2 plants, that might explain why autophagy is not entirely functional anymore. These data suggest that SH3P2 might be required during later steps of autophagosome formation, as autophagosomal structures seems to be normal during autophagy induction with AZD8055. VIGS in *N. benthamiana roq1* plants and subsequent bacterial growth measurements with *Xcv* and *Xcv ΔxopL* revealed that pTRV2-*SH3P2* plants are more susceptible towards *Xcv* (Fig. 3F). Essentially, partially reduced growth of *Xcv ΔxopL* was rescued in SH3P2-silenced plants strengthening our findings that XopL acts on *SH3P2* to suppress host autophagy and promote disease.

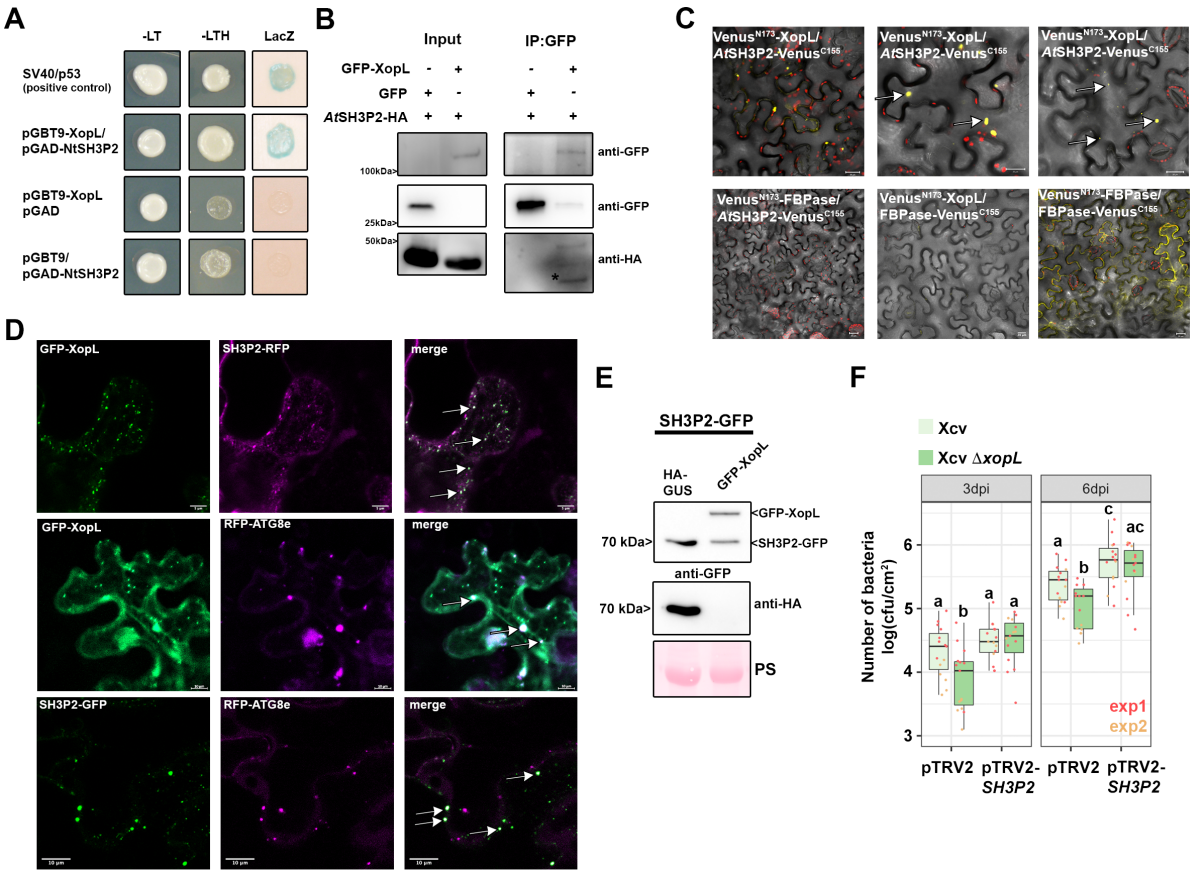


**Figure 3: XopL interacts with and degrades SH3P2 and to boost *Xcv* virulence**

**(A)** Interaction of XopL with SH3P2 in yeast two-hybrid assays. XopL fused to the GAL4 DNA-binding domain was expressed in combination with SH3P2 fused to the GAL4 activation domain (AD) in yeast strain Y190. Cells were grown on selective media before a LacZ filter assay was performed. pSV40/p53 served as positive control, while the empty AD or BD vector served as negative control. NtSH3P2 = *Nicotiana tabacum* SH3P2. –LT = yeast growth on medium without Leu and Trp, –HLT = yeast growth on medium lacking His, Leu, and Trp, indicating expression of the HIS3 reporter gene. LacZ, activity of the lacZ reporter gene.

**(B)** Coimmunoprecipitation of GFP-XopL with AtSH3P2-HA. GFP-XopL or GFP were transiently coexpressed with AtSH3P2-HA in leaves of *N. benthamiana*. After 48 h, total proteins (Input) were subjected to immunoprecipitation (IP) with GFP-Trap beads, followed by immunoblot analysis using either anti-GFP or anti-HA antibodies. AtSH3P2 = *Arabidopsis thaliana* SH3P2. Two repetitions with similar results have been conducted.

**(C)** Visualization of protein interactions *in planta* by the bimolecular fluorescence complementation assay. Yellow fluorescent protein (YFP) confocal microscopy images show *Nicotiana benthamiana* leaf epidermal cells transiently expressing Venus$^{N173}$-XopL in combination with AtSH3P2-Venus$^{C155}$. A positive control showing the dimerization of fructose-1,6-bisphosphatase (FBPase) within the cytosol. The red structures indicate autofluorescence of chloroplasts. The combination of Venus$^{N173}$-XopL with FBPase-Venus$^{C155}$ or Venus$^{N173}$-FBPase with AtSH3P2-Venus$^{C155}$ do not induce YFP fluorescence and serve as negative controls. Bars = 20 µm.

**(D)** Colocalization analysis of GFP-XopL with SH3P2-RFP, RFP-ATG8e and RFP-ATG8g in *N. benthamiana* leaves. Imaging was performed 2 d after transient expression and images represent single confocal planes from abaxial epidermal cells (scale bars = 20 µm and 10 µm, lower panel). White arrows indicate colocalization of GFP and RFP signals. The experiment was repeated twice with similar results.

383 **(E)** Total proteins were extracted 48 hpi with *A. tumefaciens* harboring the respective GFP-
384 XopL, HA-XopL and SH3P2-GFP expression constructs. SH3P2-GFP protein levels (lower
385 band) were detected using an anti-GFP antibody. Expression of the XopL was verified using an
386 anti-HA or anti-GFP antibody. Expression of GUS-HA served as a control. Ponceau S staining
387 serves as a loading control. The experiment was repeated three times with similar results.
388 **(F)** Growth of Xcv *and* Xcv *ΔxopL* strains in *roq1 N. benthamiana* plants silenced for SH3P2
389 (pTRV2-*SH3P2*) compared to control plants (pTRV2). Leaves were dip-inoculated with a
390 bacteria suspension at $OD_{600}$ = 0.2 and bacteria were quantified at 3 and 6 dpi. Red and yellow
391 data points indicate experimental repeats. Different letters indicate statistically different groups
392 ($P < 0.05$) as determined by one way ANOVA.
393
394 ***XopL mediates proteasomal degradation of SH3P2 via its E3 ligase activity***
395 Our results so far suggest that XopL might manipulate autophagy by interacting and degrading
396 the autophagy component SH3P2. Previous research on SH3P2 revealed that RNAi-mediated
397 downregulation of AtSH3P2 affects the autophagy pathway (Zhuang *et al*, 2013). To
398 understand how SH3P2 is degraded by XopL we analyzed the degradation mechanisms in more
399 detail. Firstly, degradation of AtSH3P2 by XopL was dependent on a functional proteasome, as
400 chemical inhibition of the proteasome with MG132 partially restored AtSH3P2-GFP protein
401 levels (Fig. 4A). Changes in SH3P2 protein levels were due to post-transcriptional events, as
402 gene expression of SH3P2 is rather induced upon transient expression of XopL in *N.*
403 *benthamiana,* (Fig S10A). To assess whether the proteasome-mediated degradation of SH3P2
404 was directly mediated by XopL and its E3 ligase activity, we performed an *in vitro*
405 ubiquitination assay. In the presence of all required components of the E1-E2-E3 system, we
406 observed that GST-XopL ubiquitinated MBP-AtSH3P2, which is indicated by a laddering
407 pattern, leading to larger sized molecular species of MBP-AtSH3P2, when probed with the anti-
408 MBP antibody (Fig. 4B). To address whether E3 ligase activity of XopL is crucial in the SH3P2-
409 dependent modulation of host autophagy, we employed the triple point mutant of $XopL_{H584A}$
410 $_{L585A\ G586E}$ (hereafter referred to as XopL ΔE3), lacking E3 ligase activity (Singer *et al*, 2013;
411 Erickson *et al*, 2018). Transient co-expression revealed that XopL requires its E3 ligase activity
412 to trigger the degradation of AtSH3P2 in *N. benthamiana* (Fig. 4C). This was not due to an
413 altered localization of XopL ΔE3, as it still co-localizes with AtSH3P2 upon transient
414 expression in *N. benthamiana* (Fig. S11A). In addition, XopL ΔE3 was also unable to
415 ubiquitinate SH3P2 in an *in vitro* ubiquitination assay (Fig. S11B). Consistent with its inability
416 to degrade SH3P2 *in planta*, XopL ΔE3 did not lead to a suppression of autophagy responses
417 in the quantitative luciferase autophagy assay and increase in ATG8 protein levels (Fig. 4D and
418 E). XopLΔE3 is also more unstable than XopL WT, suggesting that its E3 ligase activity is
419 crucial to maintaining its stability, likely through its function in subverting autophagy (Fig. 4F).
420 Taken together, our findings support the notion that the E3 ligase activity of XopL as well as
421 its ability to directly ubiquitinate and degrade AtSH3P2 promote suppression of autophagy.
422

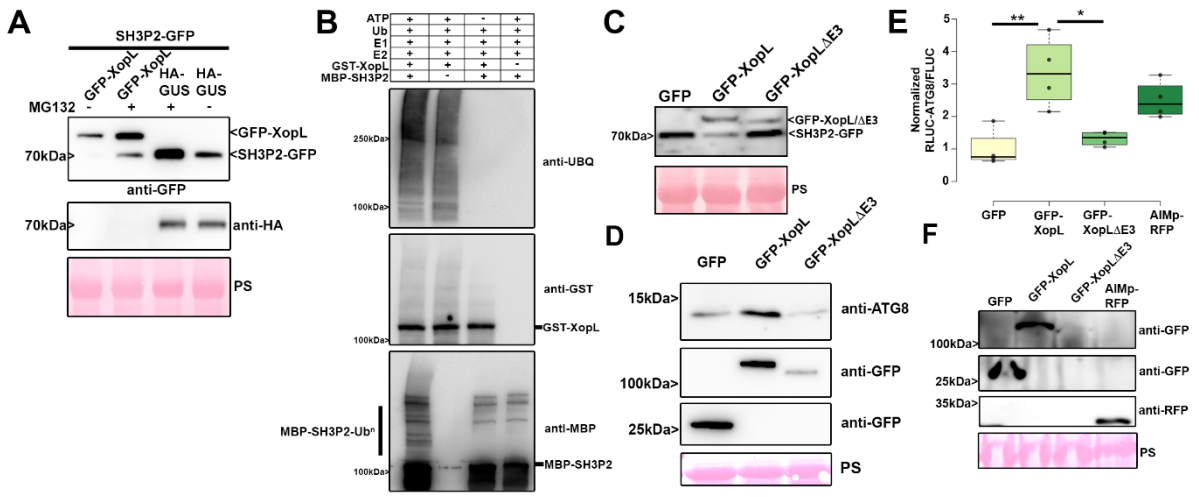


**Figure 4. XopL mediates the proteasome degradation of SH3P2 via its E3 ligase activity**

**(A)** SH3P2-GFP was transiently coexpressed together with GUS-HA and GFP-XopL in *N. benthamiana* using agroinfiltration. At 42 hpi, 200 μM MG132 was infiltrated into *A. tumefaciens*-inoculated leaves, and leaf material was collected 48 hpi. Expression of SH3P2-GFP (lower band) and GFP-XopL (upper band) was detected using an anti-GFP antibody. GUS-HA expression was confirmed with an anti-HA antibody. Ponceau S staining serves as a loading control. The experiment was repeated three times with similar results.

**(B)** *In vitro* ubiquitination assay reveals ubiquitination of SH3P2 by XopL. GST-XopL, and MBP-SH3P2 were tested using the Arabidopsis His-AtUBA1 and His-AtUBC8. Lanes 2 to 4 are negative controls. Proteins were separated by SDS-PAGE and detected by immunoblotting using the indicated antibodies. The experiment was repeated twice with similar results.

**(C)** SH3P2-GFP was transiently coexpressed together with GFP, GFP-XopL and GFP-XopL ΔE3 in *N. benthamiana* using agroinfiltration. GFP protein levels were detected with an anti-GFP antibody. Ponceau S staining serves as a loading control. The experiment was repeated three times with similar results.

**(D)** Immunoblot analysis of ATG8 protein levels in *N. benthamiana* plants transiently expressing GFP-XopL, GFP-XopL ΔE3 or GFP control at 2dpi. Expression of binary constructs was verified with an anti-GFP antibody. Ponceau Staining (PS) served as a loading control. The experiment was repeated twice with similar results.

**(E)** RLUC-ATG8a constructs were coexpressed with internal control FLUC in *N. benthamiana*. GFP-XopL, GFP-XopL ΔE3 or GFP control were co-infiltrated together with RLUC/FLUC mixture. *Renilla* and *Firefly* luciferase activities were simultaneously measured in leaf extracts at 48 hpi using the dual-luciferase system. Values represent the ratio of RLUC-ATG8a and FLUC activities (n=4). Statistical significance (* $P < 0.5$, ** $P < 0.01$) was revealed by Student's *t*-test. The experiment was repeated 3 times. Expression of proteins was verified with indicated antibodies.

***NBR1/Joka2-mediated selective autophagy degrades ubiquitinated XopL***

While we investigated the effect of *Xcv* and its T3E XopL on host autophagy, we noticed that NBR1/Joka2 responds at both transcript and protein levels during infection (Fig. 1B, 1D). We also observed that XopL protein accumulated under ConA treatment (Fig. 2C, Fig S5A), hinting that it was subject to autophagic degradation. Previous studies imply that NBR1/Joka2 mediates xenophagy by degrading viral particles, and that Joka2 is required for immunity against bacteria and *Phytophthora* (Üstün *et al*, 2018; Dagdas *et al*, 2016; Hafrén *et al*, 2018). However, the role of NBR1-mediated xenophagy in plant-*Phytophthora* and plant-bacteria interactions

461 remains unknown. Plant NBR1 is a hybrid of the mammalian autophagy adaptors NBR1 and
462 p62/SQSTM1 (Svenning *et al*, 2011). The latter was shown to mediate xenophagy of
463 *Mycobacterium tuberculosis* (Mtb) by binding to the Mtb ubiquitin-binding protein Rv1468c
464 and ubiquitin-coated *Salmonella enterica* in human cells (Chai *et al*, 2019; Zheng *et al*, 2009).
465 To corroborate our previous finding that XopL accumulates when autophagy is blocked, we
466 coexpressed GFP-XopL with autophagy inhibitor AIMp-RFP in *N. benthamiana leaves*.
467 Immunoblot analysis revealed that indeed XopL also accumulates in the presence of autophagy
468 inhibitor AIMp (Fig. 5A). As NBR1/Joka2 bodies were substantially induced during *Xcv*
469 infection (Fig. S6), and block of autophagic degradation using ConA caused accumulation of
470 GFP-XopL in vacuoles of *A. thaliana* (Fig. S12), we decided to examine whether XopL and
471 NBR1/Joka2 associate *in planta*. Intriguingly, we discovered that XopL co-localizes with
472 NBR1/Joka2 in puncta (Fig. 5B). Association of both proteins was determined using Förster
473 resonance energy transfer by fluorescence lifetime imaging microscopy (FRET-FLIM). Only
474 in the presence of RFP-XopL a significant reduction of 0.1 ns in the lifetime of the donor Joka2
475 was observed in comparison to co-expression of RFP or donor alone (Fig. 5C). This reduction
476 of lifetime is similar to what was achieved with the positive control GFP-Joka2/RFP-ATG8e.
477 These findings prompted us to investigate whether XopL might be targeted by NBR1/Joka2 for
478 autophagic degradation, similar to insoluble ubiquitinated protein aggregates (Zhou *et al*,
479 2013). Performing pull-down experiments with GFP-XopL, we discovered that XopL
480 associates with NBR1/Joka2 *in planta* (Fig. 5D), confirming the results of our FRET-FLIM and
481 co-localization studies. To address whether E3 ligase activity of XopL is required for
482 interaction, we employed XopL ΔE3, lacking E3 ligase activity. Co-IP experiments revealed
483 that XopL ΔE3 was also able to pull-down NBR1/Joka2 after transient expression in *N.*
484 *benthamiana* (Fig. 5E). This suggests that NBR1/Joka2 may not mediate the degradation of a
485 complex containing XopL and its ubiquitinated target protein(s), but rather targets XopL for
486 autophagic degradation. Given the fact that XopL is degraded by autophagy and associates with
487 NBR1/Joka2, we next analyzed stability of XopL in Joka2-silenced *N. benthamiana* plants.
488 Silencing of NBR1/Joka2 was confirmed by qPCR (Fig. S13A). Indeed, we could observe an
489 increase in GFP-XopL protein abundance (Fig. 5F), but not for GFP (Fig. S13B), in pTRV2-
490 Joka2 plants, arguing for a direct participation of NBR1/Joka2 in XopL turnover. To assess
491 whether this might impact pathogenicity of *Xcv* we performed bacterial growth assays using the
492 pTRV2-Joka2 plants. Increased growth at 3 dpi of *Xcv ΔxopQ* in *N. benthamiana* plants silenced
493 for *Joka2* strengthened our finding that Joka2 is having anti-bacterial effects on *Xcv* early on
494 during infection (Fig. 5G). As NBR1/Joka2 or p62 recognize their cargos by their ability to
495 bind ubiquitinated substrates, we hypothesized that XopL might be ubiquitinated *in planta*. To
496 test this, we transiently expressed GFP-XopL in *N. benthamiana* leaves and then
497 immunoprecipitated GFP-XopL from leaf protein extracts. Ubiquitinated GFP-XopL was
498 detected using immunoblotting. GFP-XopL, but not the GFP control, displayed
499 polyubiquitination *in planta*, while GFP-XopL ΔE3 showed reduced polyubiquitination (Fig.
500 5H). To further confirm the ubiquitination of XopL, we purified total ubiquitinated proteins
501 using the ubiquitin pan selector, which is based on a high-affinity single domain antibody that
502 is covalently immobilized on cross-linked agarose beads. We detected a smear of high-
503 molecular weight bands including the full-length XopL protein (Fig. 5I), which was strongly
504 enhanced when we co-expressed with AIMp but absent in the GFP control (Fig. S14)
505 To identify ubiquitinated residues within the XopL protein, we immunoprecipitated GFP-XopL
506 from *N. benthamiana* leaves transiently expressing GFP-XopL and performed mass
507 spectrometry (MS) analysis. *In planta* MS analysis revealed one potential ubiquitination site at
508 lysine 191 (K191) in the N-terminal part of XopL (Fig. S15A). For plant E3 ligases such as
509 PUB22, it has been reported that its stability is dependent on its autoubiquitination activity
510 (Furlan *et al*, 2017). Using MBP-XopL in an *in vitro* ubiquitination assay we confirmed self-
511 ubiquitination (Fig. S15B), indicated by the presence of higher molecular weight bands probing

512 with an anti-MBP antibody. Preforming LC-MS/MS we did detect the same ubiquitination
513 (K191) site identified *in planta* when we analyzed *in vitro* ubiquitination samples containing
514 GST-XopL (Fig. S15C). Additionally, an *in vitro* self-ubiquitination assay comparing XopL
515 WT to its K191A mutant counterpart shows that K191A displays less intensity on its high
516 molecular weight smear, suggesting that K191A is less ubiquitinated in this assay (Fig. S16A).
517 This strongly argues for K191A being an autoubiquitination site of XopL. This is strengthened
518 by our findings showing that the mutation of lysine 191 to alanine (K191A) rendered the XopL
519 K191A more stable than WT XopL (Fig. 5J) without altering its subcellular localization (Fig.
520 S16B). Changes in XopL vs. K191A protein levels were due to post-transcriptional events, as
521 gene expression of XopL and XopL K191A are similar upon transient expression in *N.*
522 *benthamiana* (Fig S16C) but did not abolish ubiquitination of XopL and association with
523 autophagic machinery as shown by co-IP with NBR1/Joka2 (Fig. 5K, Fig. S16D). However,
524 we cannot rule out trans-ubiquitination by plant E3 ligases, as XopL ΔE3 still interacts with
525 NBR1 and is still ubiquitinated in *planta*. Immunoblot analysis also revealed that XopL ΔE3 is
526 more unstable compared to XopL WT and degraded by autophagy, as it is not able to block
527 autophagy (Fig S17). This might indicate the presence of additional ubiquitination sites in
528 XopL. Taken together, our results suggest that XopL is ubiquitinated *in planta* and subjected to
529 NBR1/Joka2-dependent selective autophagy.
530

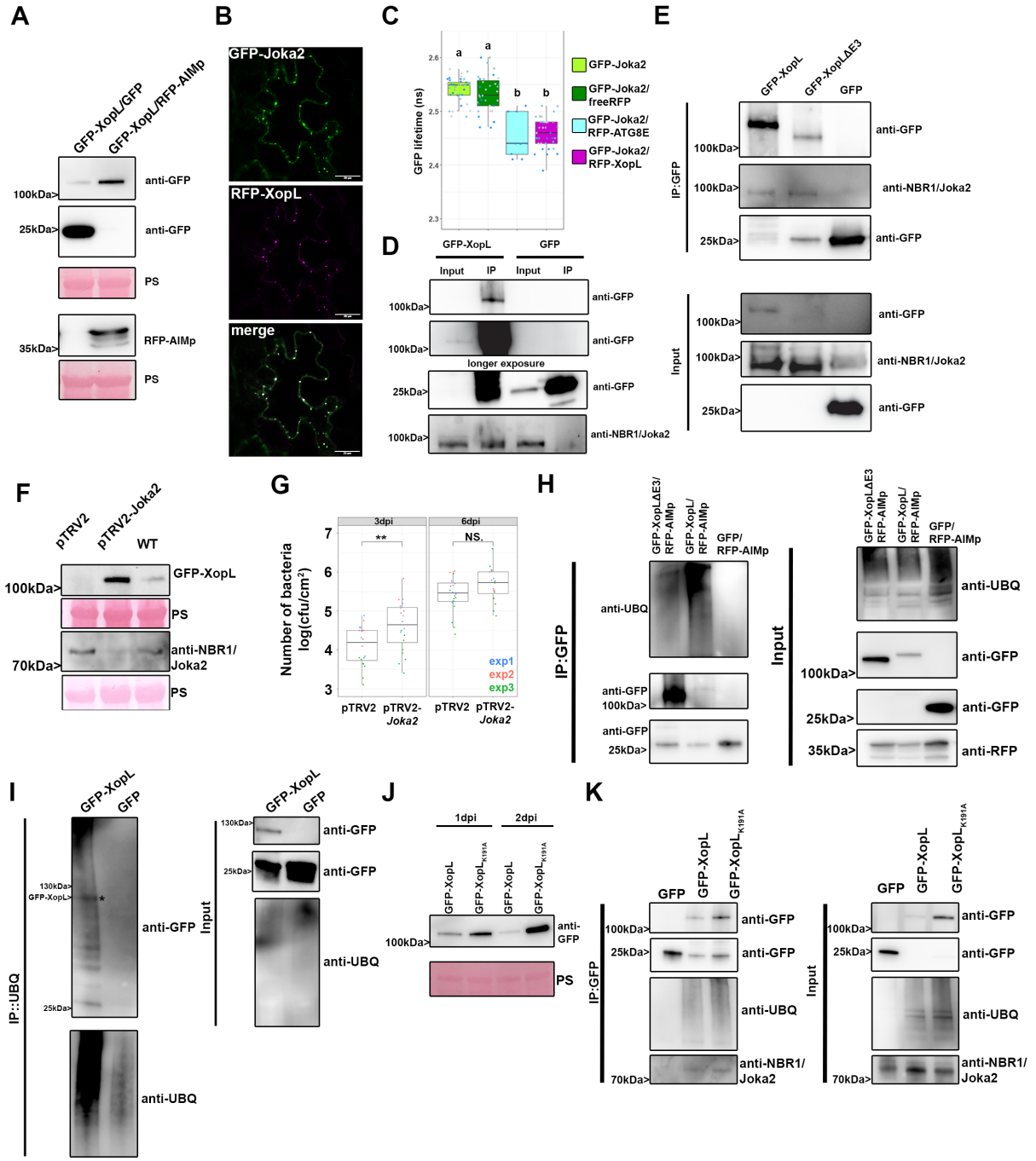


**Figure 5: XopL is ubiquitinated in planta and degraded by NBR1-mediated selective autophagy**

**(A)** GFP-XopL was coexpressed with GFP or AIMp-RFP. Proteins were separated by SDS-PAGE and detected by immunoblotting using the indicated antibodies. Ponceau Staining (PS) served as a loading control. The experiment was repeated three times with similar results.

**(B)** Colocalization of GFP-XopL with RFP-Joka2 in *N. benthamiana* leaves. Imaging was performed 2 d after transient expression and images represent single confocal planes from abaxial epidermal cells (bars = 20 µm). The experiment was repeated twice with similar results.

**(C)** FRET FLIM measurements of GFP-Joka2 and RFP-XopL in *N. benthamiana* leaves. The freeRFP construct served as a negative control and RFP-ATG8E (n = 9) as a positive control. Scattered points show individual data points, color indicates biological repeats. The lifetime (in ns) of GFP-Joka2 (donor, n = 41) was significantly reduced in the presence of RFP-XopL (n =

545 40) but not in the presence of freeRFP (n = 35). Significant differences were calculated using
546 Wilcoxon rank sum test, with significantly different groups denoted by different letters. The
547 experiment was repeated three times with similar results.
548 **(D)** Immunoprecipitation (IP) of GFP-XopL reveals association with NBR1. Immunoblots of
549 input and IP samples from *N. benthamiana* plants transiently expressing GFP or GFP-XopL
550 were probed with anti-GFP and anti-NBR1 antibodies.
551 **(E)** Immunoprecipitation (IP) of GFP-XopL and GFP-XopL ΔE3 reveals association with
552 NBR1. Immunoblots of input and IP samples from *N. benthamiana* plants transiently
553 expressing GFP, GFP-XopL and GFP-XopL ΔE3 were probed with anti-GFP and anti-NBR1
554 antibodies.
555 **(F)** GFP-XopL was transiently expressed in pTRV2, pTRV2-Joka2 and *N. benthamiana* WT
556 plants. Expression of binary constructs was verified with an anti-GFP antibody. Joka2 silencing
557 was verified using an anti-NBR1 antibody. Ponceau Staining (PS) served as a loading control.
558 The experiment was repeated twice with similar results.
559 **(G)** Growth of Xcv *ΔxopQ* in *N. benthamiana* plants silenced for *Joka2* (pTRV2-Joka2)
560 compared to control plants (pTRV2). Leaves were dip-inoculated with a bacteria suspension at
561 $OD_{600}$ = 0.2. and bacteria were quantified at 3 and 6 dpi. Red, blue, and green data points
562 represent repeats of the experiments. Significant differences were calculated using Student's *t-*
563 *test* and are indicated by: **, $P < 0.01$. The experiment was repeated three times with similar
564 trends.
565 **(H)** GFP-XopL, GFP-XopL ΔE3 were transiently expressed in *N. benthamiana*. RFP-AIMp
566 was co-infiltrated to stabilize both XopL variants. Samples were taken 48 hpi, and total proteins
567 (Input) were subjected to immunoprecipitation (IP) with GFP-Trap beads, followed by
568 immunoblot analysis of the precipitates using either anti-GFP or anti-ubiquitin antibodies. GFP
569 served as a negative control. RFP-AIMp expression was verified by an anti-RFP antibody. The
570 experiment was repeated three times with similar results.
571 **(I)** GFP-XopL was transiently expressed in *N. benthamiana*. Samples were taken 48 hpi, and
572 total proteins (Input) were subjected to immunoprecipitation (IP) with the ubiquitin pan
573 selector, followed by immunoblot analysis of the precipitates using either anti-GFP or anti-
574 ubiquitin antibodies. GFP served as a control. Asterisk indicates the GFP-XopL full-length
575 protein. The experiment was repeated two times with similar results.
576 **(J)** Immunoblot analysis GFP-XopL and GFP-$XopL_{K191A}$ at 1 and 2 dpi using an anti-GFP
577 antibody. Ponceau Staining (PS) served as a loading control. The experiment was repeated three
578 times with similar results.
579 **(K)** GFP-XopL and GFP-$XopL_{K191A}$ were transiently expressed in *N. benthamiana*. Samples
580 were taken 48 hpi, and total proteins (Input) were subjected to immunoprecipitation (IP) with
581 GFP-Trap beads, followed by immunoblot analysis of the precipitates using either anti-GFP,
582 anti-ubiquitin and anti-NBR1 antibodies. GFP served as a control. The experiment was repeated
583 three times with similar results.
584

585 ## Discussion

586

587 Here, by studying *Xanthomonas*-host interactions, we revealed a complex multi-layered
588 regulatory role of autophagy in plant immunity. We demonstrate that *Xanthomonas* can subvert
589 plant autophagy which is achieved by the T3E XopL. Through its E3 ligase activity, XopL can
590 ubiquitinate and degrade SH3P2, an autophagy component functioning in autophagosome
591 biogenesis. This in turn dampens autophagy to boost the virulence of Xanthomonas. However,
592 the same T3E is targeted by NBR1/Joka2-triggered selective autophagy/xenophagy which
593 constitutes a novel form of plant defense mechanism (Fig. 6). The mutual targeting of pathogen

effector XopL and plant protein SH3P2 unveils how different layers of regulation contribute to autophagy pathway specificity during host-bacteria interactions.

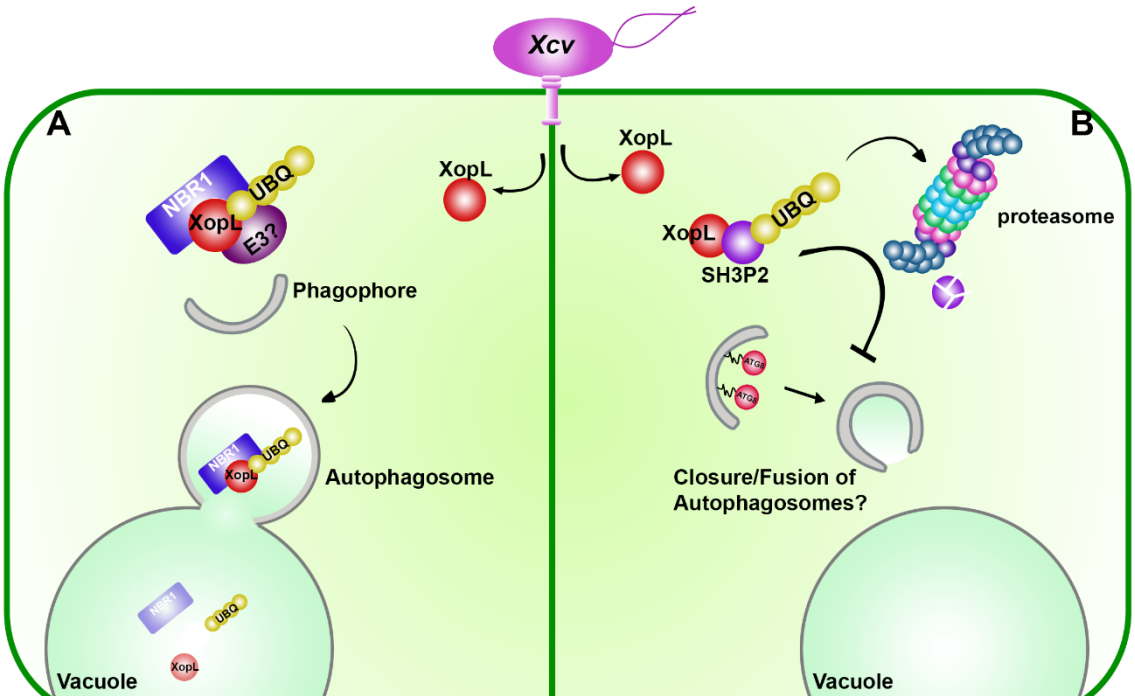


**Figure 6: Model illustrating the function of XopL**
**(A) Xenophagy of XopL:** Upon delivery of XopL in the plant XopL undergoes self-ubiquitination and possible ubiquitination by an unknown host E3 ligase. Joka2/NBR1 associates with XopL and triggers its degradation via the selective autophagy pathway in the vacuole. **(B) XopL blocks autophagy**: XopL interacts with autophagy component SH3P2 inside the cell and ubiquitinates it to degrade it via the 26S proteasome. Degradation of SH3P2 results in defects of autophagosome delivery into the vacuole and hence suppresses autophagy.

*Autophagy in host-immune interactions*

In animals, several pathogenic bacteria have been identified to modulate the autophagy pathway to their own benefit (Huan & Brummel, 2014). Many intracellular animal pathogenic bacteria can be eliminated by autophagy, while others (such as *Shigella*, *Yersinia* and *Listeria*), are able to exploit autophagy to increase their pathogenicity (Huan & Brummel, 2014). In plants, several studies have highlighted that pathogens manipulate the autophagy pathway (Leary *et al*, 2018). More specifically, the plant pathogenic bacterium *Pseudomonas syringae* pv. *tomato* (*Pst*) has been shown to utilize effectors to modulate autophagic degradation (Üstün *et al*, 2018; Üstün *et al*, 2016). With *Xcv,* we have identified another plant pathogenic bacterium that modulates autophagy, similar to *Pst*, in an effector-dependent manner. Although, both pathogens have the same habitat and hemi-biotrophic lifestyle, they act in different ways on the autophagy pathway. For *Xcv* inhibition of the autophagy pathway is crucial to maintain pathogenicity while *Pst* activates it for its own benefit (Üstün *et al*, 2018). Previously, it has been reasoned that autophagy activation might be essential to maintain plant viability and lifespan (Hafrén *et al*, 2018). However, autophagy may not be required for this during *Xcv* infection, as it has been shown that T3Es XopD and XopJ are able to prolong the biotrophic phase by other mechanisms (Üstün et al, 2013; (Kim *et al*, 2008). As such, autophagy is dispensable for the virulence of *Xcv* and actively dampened to boost virulence and partially prevent xenophagy of XopL. Within the realm of xenophagy, the degradation of effectors by autophagy can be considered as a form of "effectorphagy". Perturbation of general autophagy is achieved by degrading SH3P2 through

627 the action of T3E XopL. SH3P2 was first identified as a novel autophagy component,
628 stimulating autophagosome formation during nitrogen starvation and BTH-triggered immune
629 responses (Zhuang *et al*, 2013). Later studies also showed that SH3P2 plays a key role in
630 membrane tubulation during cell plate formation (Ahn *et al*, 2017) and clathrin-mediated
631 endosomal sorting and degradation, with no effect in dark-induced autophagy (Nagel *et al*,
632 2017). Our findings that silencing of SH3P2 from *N. benthamiana* impairs autophagy and
633 somewhat promotes pathogenicity sheds further light on its diverse functions. However, the
634 effects of XopL on SH3P2 and increasing virulence of *Xcv* might not only be attributed to its
635 function in autophagy. Because endocytic trafficking also plays a major role in plant immunity
636 (Gu *et al*, 2017), it is likely that XopL has a function beyond autophagy to impair plant defense
637 mechanisms. This is also supported by the fact that XopL can reduce PTI responses (Singer *et*
638 *al*, 2013), which is not due its function in autophagy, as autophagy deficiency has no impact on
639 PTI responses (Lenz *et al*, 2011). Previously, XopL was also shown to impact stromule
640 formation by localizing to microtubules (Erickson *et al*, 2018), which was shown only for the
641 XopL version lacking E3 ligase activity. Although, we do not see any microtubule localization
642 of the XopL ΔE3 version, XopL might affect stromule formation as they are thought to be
643 recognized by autophagic membranes prior autophagic degradation (Marshall & Vierstra,
644 2018).
645 *Role of xenophagy in immunity*
646 One of the best studied selective autophagy receptors across kingdoms is NBR1/p62 that plays
647 a central role in xenophagy and degradation of protein aggregates (Kirkin *et al*, 2009; Svenning
648 *et al.*, 2011). Its role in plant immune responses has been shown by the involvement of
649 NBR1/Joka2-mediated selective autophagy in restricting pathogen growth or disease
650 progression during *P. infestans* or *Pst* infection (Üstün *et al*, 2018, Dagdas *et al*, 2016). In
651 animals, p62, the counterpart of plant NBR1, functions to mediate xenophagy, which has been
652 also described for NBR1 in plants in a plant-virus infection context but not for other plant
653 pathogens (Hafrén et al, 2017, Hafrén *et al*, 2018). Our analysis provides the first evidence that
654 like viral proteins, bacterial effector XopL constitutes a target of NBR1-mediated selective
655 autophagy. This sheds light on previous findings about the role of NBR1/Joka2 in plant
656 immunity and makes it a central hub in plant-microbe interactions. Consequently, XopL
657 developed the ability to suppress autophagy, to boost the virulence of Xcv. But does XopL
658 suppress autophagy to an extent to escape its own degradation? Indeed, treating plants with
659 ConA or expressing AIMp still stabilize XopL protein levels, indicating that the effect of XopL
660 on the autophagy pathway is either very specific or not sufficient to shut down the pathway
661 completely. It is also possible that XopL is degraded by other additional mechanisms such as
662 endocytosis or proteasome-mediated degradation as it most likely ubiquitinated by plant E3
663 ligases. In line with our observations on the autophagy pathway is that the ability of XopL to
664 suppress the autophagy is still less than the recently discovered autophagy inhibitor AIMp
665 (Pandey *et al*, 2021). This is also in line with the fact that loss of SH3P2 is only partially
666 suppressing autophagy formation (Zhuang *et al*, 2013) while silencing of ATG7 or expression
667 of AIMp result in a complete block of autophagy. Currently, we also do not know whether
668 SH3P2 might only affect a subset of ATG8 isoforms to facilitate autophagosome formation.
669 Thus, it might be also possible that the NBR1/Joka2-selective autophagy pathway might
670 involve ATG8 isoforms that do not require SH3P2.
671
672 To date, it has not been reported that bacterial effectors in animals and plants are removed by
673 selective autophagy as an anti-microbial response. Interestingly, the *Salmonella* effector SseL,
674 which inhibits selective autophagy to abolish p62-dependent degradation of *Salmonella*, was
675 also found to interact with p62 (Mesquita *et al*, 2012). This might suggest the possibility that
676 SseL might also have been an autophagy target before it acquired its function to block this
677 pathway via its deubiquitinase activity (Mesquita *et al*, 2012). We hypothesize that NBR1/p62

might have evolved to have a function in anti-bacterial autophagy by triggering xenophagy of bacterial molecules as an alternative strategy to degrade entire intracellular bacteria. This may have happened for the function of NBR1 in plants, as fungal and oomycete pathogens as well as Gram-negative bacteria reside in the extracellular space. Animal pathogens also occupy the extracellular space, before entering the host cell. In the case of *Salmonella*, it first needs to inject bacterial effectors via its SPI-1 T3SS to establish internalization and its replication niche (Lou *et al*, 2019). It is therefore tempting to speculate that these effectors may be targeted by selective autophagy mechanisms as an early defense mechanism of the immune system. Similar to XopL, several of the SPI1 T3Es can mimic E3 ligases and/or are ubiquitinated in the host cell (Kubori & Galan, 2003), making them potential targets for NBR1/p62-mediated selective autophagy. Indeed, T3Es SopA and SopE have been reported to be degraded through the proteasome (Kubori & Galan, 2003; Zhang *et al*, 2005). A possible degradation by autophagy was not investigated in these studies. Our results also suggest that XopL is targeted by a host E3 ligase for degradation as the XopL variant lacking E3 ligase activity is still ubiquitinated *in planta* and degraded by autophagy. Several E3 ligases have been implicated in plant-microbe interactions, which opens up the possibility that they may target microbial proteins (Furlan *et al*, 2012).

Although plant pathogenic bacteria possess T3Es that are implicated in the host ubiquitin system, to date there is no evidence that they might be ubiquitinated in the host. In addition, we identified that XopL undergoes self-ubiquitination, which has not been reported for animal and plant pathogenic bacterial effectors.
In this scenario, it is tempting to speculate whether the self-ubiquitination activity of XopL attracts it to the autophagy pathway. Although the biological significance of K191 remains elusive, it might still have regulatory functions. To date, self-ubiquitination of E3 ligases has been assigned as a mechanism of self-regulation through which their activity is controlled (Furlan *et al.*, 2017). In the case of bacterial T3Es that mimic E3 ligases, it might be a strategy to trick degradation systems. Other post-translational modifications of T3Es such as phosphorylation of AvrPtoB have been found to crucial for its virulence function (Lei *et al*, 2020), which might be also the case for the ubiquitination of XopL. Our results suggest that ubiquitinated XopL is targeted for autophagic degradation which might be indeed a strategy to recruit different autophagy components. Indeed, we can find a high conservation of K191 in several other XopL-like T3Es across different Xanthomonas species (Fig S18), which would be in favor of the proposed hijacking hypothesis. However, the fact that the K191 variant is still ubiquitinated *in planta* and associates with NBR1 and other autophagy components are not in favor of this hypothesis. The discovery of other alternative ubiquitination sites in XopL will help us to unravel why XopL undergoes self-ubiquitination and how this might contribute to its virulence.

Taken together, we provide a primary example where a bacterial effector subverts host autophagy to downregulate host immunity, and the autophagic machinery in turn targets the same bacterial effector for degradation. Thus, this reveals a complex multi-layered role of autophagy particularly in the context of immunity and disease. Additionally, XopL possesses self-ubiquitination activity, which some evidence we have uncovered here suggest that this functions to hijack the host autophagy system.

## Acknowledgements

We thank Ingrid Schießl for the initial Y2H screen with XopL. We also thank Tom Denyer for critical reading of the manuscript. We thank Johannes Stuttmann for the *roq1 N. benthamiana* seeds. We thank Silke Wahl and Irina Droste-Borel for technical support for the proteomics assay. This work was supported by an Emmy Noether Fellowship GZ: UE188/2-1 from the

Deutsche Forschungsgemeinschaft (DFG; to S.Ü.), and through the collaborative research council 1101 (SFB1101; to G.L.). E.A.M. was supported by EU Horizon 2020 MSCA IF (799433). F.B. was supported by funds from the DFG (BO1961/5-2). D.H. was supported by grants from the Swedish research councils VR (2016-04562; 2020-05327) and FORMAS (2017-01596). T.O.B. was supported by BBSRC - Biotechnology and Biological Sciences Research Council, grant code BB/T006102/1. M.B.M. was supported by NSF IOS Grant 2026368. FORMAS (grant number 2016-01044) for A.H. We thank the confocal microscopy facility of ZMBP that is supported by funds from DFG (INST 37/819-1 FUGG and INST 37/965-1 FUGG), especially Sandra Richter and Natalie Krieger for their introduction into the Zeiss LSM880, Leica SP8 and FRET-FLIM.

# Material and Method

### Plant Material and Growth Conditions

Wild-type plants were *Arabidopsis thaliana* ecotype Columbia (Col-0) and *Nicotiana benthamiana. Arabidopsis* plants were grown on soil under short-day conditions (8/16-h light/dark cycles) in a growth chamber or for maintenance and crossings under long-day conditions (16/8-h light/ dark cycles) in a growth room with light intensity of 150 µE, 21°C, and 70% relative humidity, respectively. *N. benthamiana* plants were grown under long day conditions 16/8-h light/dark cycles, 21°C, and 70% relative humidity.

### Plasmid construction

For transient expression experiments, the coding region of XopL, AtSH3P2 or SlJoka2 were cloned into pENTR/D-TOPO and subsequently recombined into pUBN-DEST-GFP or RFP (Grefen *et al*, 2010), pGWB614/5 (Nakagawa *et al*, 2007), pMAlc2, pDEST15. The RFP-ATG8E/G, GFP-ATG8e, RFP-NBR1, RLUC-ATG8, RLUC-NBR1, XopD-GFP, XopJ-GFP, pTRV2-Joka2, pTRV2-ATG7 constructs were described previously (Üstün *et al,* 2018, Üstün *et al*, 2013). All binary plasmids were transformed into Agrobacterium tumefaciens strain C58C1 and infiltration of *N. benthamiana* was done at the four-to six-leaf stage. Stable Arabidopsis transformation was performed using the floral dip method (Clough & Bent, 1998).

### Transient Expression in *N. benthamiana* by Agrobacterium-Mediated Leaf Infiltration

Transient expression was performed as described previously (Üstün *et al*, 2018).

### Immunoprecipitation

GFP pull-down assays were performed as previously described (Üstün *et al*, 2018. Pulldown of ubiquitinated proteins was performed according to manufacturer's instructions (NanoTag Biotechnologies).

### *In vitro* pull-down

In vitro pull-down was performed as previously described (Üstün *et al*, 2013).

### Dual Luciferase Assay

Dual luciferase assay was performed as described previously (Üstün *et al*, 2018).

### Virus-induced gene silencing

VIGS was performed as described previously (Üstün *et al*, 2013).

### Bacterial growth conditions

*Agrobacterium tumefaciens*, Agrobacteria strain C58C1 was grown in LB Hi-Salt (10g/L sodium chloride, 10g/L tryptone, 5g/L yeast extract) with 100 µg mL−1 rifampicin at 28 °C. The cultures supplemented with the appropriate antibiotics for those harboring plasmids. Xcv strain 85-10 was grown in NYG media (0.5% peptone, 0.3% yeast extract, 2% glycerol) with 100 µg mL−1 rifampicin at 28 °C.

**Construction of Xcv Δ*xopL* and Δ*xopQ* null mutants**

To construct Xcv 85-10 *xopL* and *xopQ* deletion mutants, the 1.7-kb upstream and downstream regions of the xopL or xopQ gene were PCR amplified using Xcv 85-10 genomic DNA as template and cloned into pLVC18 linearized with EcoRI (New England Biolabs) using Gibson assembly. The plasmid was introduced into Xcv 85-10 by triparental mating. Xcv transconjugants were analysed by PCR to confirm that homologous recombination occurred at the xopL or XopQ locus.

**Constructs for Xcv Δ*xopL* complementation analysis**

To construct xopL gene with 0.3-kb promoter region in broad host range vector, 0.3-kb promoter-xopL gene was PCR amplified using Xcv 85-10 genomic DNA as template and cloned into pBBR1MCS-2 (Kovach *et al*, 1995) linearized with EcoRV (New England Biolabs) using Gibson assembly. The plasmid was introduced into Xcv 85-10 Δ*xopL* by triparental mating.

**Bacterial infection**

Xcv carrying a deletion mutation of XopQ (Xcv *ΔxopQ*), or of HrcN (Xcv Δ*hrcN*), or of both XopQ and XopL (Xcv *ΔxopQ ΔxopL*) were used to infect wild-type *N. benthamiana*. Xcv were grown overnight in NYG with appropriate antibiotics at 28°C with shaking. Bacteria were diluted to $OD_{600}$ = 0.2 for dual-luciferase assays, immunoblot analysis of NBR1, ATG8 or confocal microscopy of autophagosomal structures. For in planta growth curves using syringe infiltration, Xcv strains were inoculated at $OD_{600}$ = 0.0004, and for dip-inoculation $OD_{600}$ = 0.2 was used.

**Tomato growth condition and bacterial growth assay**

Tomato (*Solanum lycopersicum*) cv. VF36 was grown in greenhouse (22-28 °C, 50-70 % RH, 16-h light). For bacterial growth assays, leaflets were dipped in a 2 x $10^8$ CFU/mL suspension of Xcv 85-10 strains in 10mM MgCl2 with 0.025% (v/v) silwet L-77 (Helena Chemical Company) for 30 sec. Plants were then placed in plastic chambers at high humidity (>95%) for 24 h. For each strain analyzed, four leaf discs (0.5 $cm^2$) per treatment per timepoint were ground in 10 mM $MgCl_2$ and diluted and spotted onto NYGA plates in triplicate to determine bacterial load. Three biological replicates (i.e., three plants) were used, and the experiment was repeated at least three times.

**Confocal Microscopy**

Live-cell images were acquired from abaxial leaf epidermal cells using a Zeiss LSM780 and LSM880 microscope. Excitation/emission parameters for GFP and RFP were 488 nm/490 to 552 nm and 561 nm/569 to 652 nm, respectively, and sequential scanning mode was used for colocalization of both fluorophores. Confocal images with ImageJ (version 2.00) software. Quantification of ATG8-labeled autophagosomal structures was done on z-stacks that were converted to eight-bit grayscale and then counted for ATG8 puncta either manually or by the Particle Analyzer function of ImageJ.

**FRET-FLIM measurement**

828 FRET-FLIM was performed on SP8 confocal laser scanning microscope (CLSM) (Leica
829 Microsystems GMBH) with LAS AF and SymPhoTime 64 software using a 63x/1.20 water
830 immersion objective. FLIM measurements were performed with a 470 nm pulsed laser (LDH-
831 P-C-470) with 40 MHz repetition rate and a reduced speed yielding, with an image resolution
832 of 256x256, a pixel dwell time of ~10 µs. Max count rate was set to ~15000 cps. Measurements
833 were stopped, when the brightest pixel had a photon count of 1000. The corresponding emission
834 was detected with a Leica HyD SMD detector from 500 nm to 530 nm by time-correlated single-
835 photon counting using a Timeharp260 module (PicoQuant, Berlin). The calculation of GFP
836 lifetime was performed by iterative reconvolution, i.e. the instrument response function was
837 convolved with exponential test functions to minimize the error with regard to the original
838 TCSPC histograms in an iterative process. For measurements of GFP-JOKA2 protein
839 aggregates, ROIs were drawn manually on SymphoTime64 software around the aggregates to
840 analyze GFP lifetime in these structures.
841
842 **Immunoblot analysis**
843 Proteins were extracted in 100 mM Tris (pH 7.5) containing 2% SDS, boiled for 10min in SDS
844 loading buffer, and cleared by centrifugation. The protein extracts were then separated by SDS-
845 PAGE, transferred to PVDF membranes (Biorad), blocked with5% skimmed milk in PBS, and
846 incubated with primary antibodies anti-NBR1 (Agrisera), anti-ATG8 (Agrisera), anti-ubiquitin
847 (Agrisera), anti-GFP (SantaCruz), anti-RFP (Chromotek), anti-HA (Sigma Aldrich) primary
848 antibodies using 1:2000 dilutions in PBS containing 0.1% Tween 20. This was followed by
849 incubation with horseradish peroxidase-conjugated secondary antibodies diluted 1:10,000 in
850 PBS containing 0.1% Tween 20. The immunoreaction was developed using an ECL Prime Kit
851 (GE Healthcare) and detected with Amersham Imager 680 blot and gel imager.
852
853 ***In vitro* ubiquitination assay**
854 Recombinant proteins were expressed in *E. coli* BL21(DE3) and purified by affinity
855 chromatography using amylose resin (New England Biolabs). Recombinant His-UBA1 and
856 His-UBC8 were purified using Ni-Ted resin (Macherey-Nagel). Purified proteins were used for
857 *in vitro* ubiquitination assays. Each reaction of 30 mL final volume contained 25 mM Tris-HCl,
858 pH 7.5, 5 mM MgCl2, 50 mM KCl, 2 mM ATP, 0.6 mM DTT, 2 µg ubiquitin, 200 ng E1 His-
859 *At*UBA1, 1.2 µg E2 His-*At*UBC8, 2 µg of E3s, and 0.3 µg of MBP-*At*SH3P2. Samples were
860 incubated for 1h at 30°C and reaction was stopped by adding SDS loading buffer and incubated
861 for 10 min at 68°C. Samples were separated by SDS-PAGE electrophoresis using 4–15% Mini-
862 PROTEAN® TGX™ Precast Protein Gels (BioRad) followed by detection of ubiquitinated
863 substrate by immunoblotting using anti-MBP (New England Biolabs), anti-GST and anti-
864 ubiquitin (Santa Cruz Biotechnology) antibodies.
865
866 **NanoLC-MS/MS analysis and data processing**
867 Proteins were purified on an NuPAGE 12% gel (Invitrogen) and Coomassie-stained gel pieces
868 were digested in gel with trypsin as described previously (Borchert *et al*, 2010) with a small
869 modification: chloroacetamide was used instead of iodoacetamide for carbamidomethylation of
870 cysteine residues to prevent formation of lysine modifications isobaric to two glycine residues
871 left on ubiquitinylated lysine after tryptic digestion. After desalting using C18 Stage tips peptide
872 mixtures were run on an Easy-nLC 1200 system coupled to a Q Exactive HF-X mass
873 spectrometer (both Thermo Fisher Scientific) as described elsewhere (Kliza *et al*, 2017) with
874 slight modifications: the peptide mixtures were separated using a 87 minute segmented gradient
875 from 10-33-50-90% of HPLC solvent B (80% acetonitrile in 0.1% formic acid) in HPLC solvent
876 A (0.1% formic acid) at a flow rate of 200 nl/min. The seven most intense precursor ions were
877 sequentially fragmented in each scan cycle using higher energy collisional dissociation (HCD)
878 fragmentation. In all measurements, sequenced precursor masses were excluded from further

879 selection for 30 s. The target values were 105 charges for MS/MS fragmentation and 3x106
880 charges for the MS scan.
881 Acquired MS spectra were processed with MaxQuant software package version 1.5.2.8 with
882 integrated Andromeda search engine. Database search was performed against a *Nicotiana*
883 *benthamiana* database containing 74,802 protein entries, the sequences of XopL from
884 *Xanthomonas campestris* pv. *vesicatoria*, and 285 commonly observed contaminants.
885 Endoprotease trypsin was defined as protease with a maximum of two missed cleavages.
886 Oxidation of methionine, phosphorylation of serine, threonine and tyrosine, GlyGly dipetide on
887 lysine residues, and N-terminal acetylation were specified as variable modifications.
888 Carbamidomethylation on cysteine was set as fixed modification. Initial maximum allowed
889 mass tolerance was set to 4.5 parts per million (ppm) for precursor ions and 20 ppm for fragment
890 ions. Peptide, protein and modification site identifications were reported at a false discovery
891 rate (FDR) of 0.01, estimated by the target-decoy approach (Elias and Gygi). The iBAQ
892 (Intensity Based Absolute Quantification) and LFQ (Label-Free Quantification) algorithms
893 were enabled, as was the "match between runs" option (Schwanhausser *et al*, 2011).
894
895 **RNA extraction and RT-qPCR**
896 RNA was extracted from 4 leaf discs according to manufacturer instructions using the
897 GeneMATRIX Universal RNA Purification Kit (Roboklon) with on-column DNase I digestion.
898 RNA integrity was checked by loading on 1% agarose gel and separating by electrophoresis.
899 RNA concentrations were measured using Nanodrop 2000 (Thermo Fisher), and equal amounts
900 of RNA were used for cDNA synthesis. cDNA synthesis was performed using LunaScript™
901 RT SuperMix Kit (New England Biolabs) and in a standard thermocycler according to
902 manufacturer instructions. Gene expression was measured by qPCR using MESA BLUE qPCR
903 MasterMix Plus for SYBR® Assay No ROX (Eurogentec) and cycle quantification by Biorad
904 CFX system.
905
906 **Drug treatments**
907 For the analysis of protein stability 200 µM MG132 or 1% EtOH was infiltrated to plants
908 transiently expressing binary constructs 2dpi. 6 hours later leaf material was harvested. were
909 analysed under the CLSM. Concanamycin A treatment was performed by syringe infiltration
910 of mature leaves with 0.5 µM ConA for 6-8 h prior confocal analysis or immunoblot analysis.
911 AZD8055 (15 µM) was done for 6-8 hours prior confocal microscopy.
912
913 **Phylogenetic Analysis**
914 An alignment between SH3P2 proteins was generated using ClustalW wand the tree was
915 generated using the neighbor-joining method. Effector proteins related to XopL were identified
916 performing a BLASTp (https://blast.ncbi.nlm.nih.gov/Blast.cgi) using XopL protein sequence
917 (ID: CAJ24951.1). 18 protein sequences were extracted from the Top100 sequences from Blast
918 results with only the top hit considered per species/pathovars. Related effectors from more
919 distant bacteria were identified realizing a second BLASTp excluding Xanthomonas genus and
920 3 proteins from relevant species were extracted from the Top10 results. Protein from
921 X*anthomonas campestris pv. Campestris* was included manually as an example of non-
922 conserved protein from Xanthomonas genus. Multiple Sequence Alignment of the 24 extracted
923 sequences was performed using COBALT
924 (https://www.ncbi.nlm.nih.gov/tools/cobalt/cobalt.cgi) from NCBI.
925
926 **Data Analysis and Presentation**
927 Data are presented as boxplots with visible datapoints, where middle horizontal bars of boxplots
928 represent the median, the bottom and top represent the 25th and 75th percentiles, whiskers
929 extend to at most 1.5 times the interquartile range. Statistical significance was analysed using

appropriate statistical tests, either by Student's t test, one way ANOVA or Kruskal-Wallis rank sum test (*P < 0.05, **P < 0.01, and P*** < 0.001). The number of biological replicates (n) is given in the figure legends. Statistical analyses and graphical presentation of data were made in R and RStudio (Version 1.2.5033). Boxplots were prepared using the ggplot2 package.

## Supporting information

**Figure S1: S**ilencing of *ATG7* in *N. benthamiana* plants abolishes autophagosome formation and Xcv blocks autophagy at 6hpi.
**Figure S2:** Virus induced gene silencing of *ATG7* in *N. benthamiana* is beneficial for Xcv.
**Figure S3:** Suppression of autophagy is enhanced by T3Es**.**
**Figure S4:** Screening for Xanthomonas T3Es with altered autophagic flux.
**Figure S5:** XopL contributes to Xcv virulence.
**Figure S6:** Joka2 bodies are induced during Xcv infection in a XopL-dependent manner.
**Figure S7:** Transgenic *A. thaliana* GFP-XopL plants display defects in autophagic degradation.
**Figure S8**: SH3P2 is conserved in different plant species.
**Figure S8:** XopL is ubiquitinated *in planta*.
**Supplemental Video 1:** XopL/SH3P2 puncta are mobile.
**Figure S9:** Silencing of SH3P2 in *N. benthamiana* perturbs autophagy.
**Figure S10:** Gene expression of SH3P2 is induced by XopL and XopL-mediated degradation is due to post-transcriptional degradation events.
**Figure S11:** RFP-XopL ΔE3 co-localizes with and is unable to ubiquitinate SH3P2-GFP.
**Figure S12:** XopL is degraded in the vacuole.
**Figure S13:** Virus-induced gene silencing of *Joka2* in *N. benthamiana* plants.
**Figure S14:** XopL in planta ubiquitination is enhanced by the presence of AIMp.
**Figure S15:** XopL is ubiquitinated *in planta* and undergoes self-ubiquitination.
**Figure S16**: Characterization of $XopL_{K191A}$ variant i*n vitro* and *in planta*.
**Figure S17:** XopL ΔE3 is degraded by autophagy.
**Figure S18:** XopL K191 residue is highly conserved through the Xanthomonas genus
**Supplemental Table 1**: Primers used in manuscript.

## Author contributions

J.X.L, S.Ü., M.R., D.S., G.L., A.R.G., J.-G.K., M.F.-W. performed the experiments. J.X.L-, M.R., G.L., E.A.M., M.F.W., B.M., A.H., T.O.B., M.B.M., F.B., D.H., and S.Ü. analysed the data. P.P. and T.O.B. provided novel material. S.Ü. planned the project and wrote the article together with J.X.L and input from all authors.

## Figure Legends

**Figure 1: Xanthomonas blocks autophagy to enhance its pathogenicity**
**(A**) RFP-ATG8g-labeled autophagosomes were quantified from plants infected with mock or Xcv *ΔxopQ* at 2 dpi in the presence or absence of ConA (bars = 20 µm). Puncta were calculated from z-stacks (15) of *n*=6 individuals using ImageJ. Data points are plotted as open circles. Different letters indicate statistically significant differences ($P < 0.05$) as determined by one-way ANOVA. The experiment was repeated twice with similar results.
**(B)** Immunoblot analysis of NBR1 and ATG8 protein levels in Xcv *ΔxopQ* or mock infected *N. benthamiana* plants at 1 and 2dpi. Agrobacterium-mediated transient expression of AIMp-RFP

978 serves as a control for autophagy suppression. Ponceau Staining (PS) served as a loading
979 control. The experiment was repeated three times with similar results.
980 **(C)** RLUC-ATG8a or RLUC-NBR1 constructs were coexpressed with internal control FLUC
981 in *N. benthamiana*. *Xcv ΔxopQ* was co-infiltrated with Agrobacteria containing the luciferase
982 reporter constructs. Coexpression of RFP-AIMp serves as a control for autophagy inhibition.
983 Expression of the latter was confirmed with western blot (inset). *Renilla* (RLUC) and *Firefly*
984 (FLUC) luciferase activities were simultaneously measured in leaf extracts at 48 h post-
985 infiltration using the dual-luciferase system (n=4). Statistical significance (***$P$<0.001) was
986 revealed by Student's *t*-test. The experiment was repeated more than 3 times with similar
987 results.
988 **(D)** RT-qPCR analysis of *NbATG8-1.1/1.2, NbATG8-2.1/2.2* and *NbJoka2* transcript levels
989 upon challenge of *N. benthamiana* plants with Xcv *ΔxopQ* for 1 and 2 dpi compared to mock
990 infected plants. Values represent expression relative to mock control of respective time point
991 and were normalized to *actin*. Statistical significance (*$P$ < 0.05, **$P$ < 0.01, *** $P$ < 0.001)
992 was revealed by Student's *t*-test.
993 **(E)** Bacterial density in leaves of *N. benthamiana* infected with *Xcv* in the presence or absence
994 autophagy suppressor AIMp-RFP. Leaves were syringe-infiltrated with $OD_{600}$ = 0.0004, and
995 colony-forming units were counted at 6 dpi. Compared to empty vector control (EV), AIMp
996 expressing plants (n=6) harbour significantly more bacteria. Bacterial growth was repeated with
997 the same result in 12 plants over two independent experiments. Red and yellow data points
998 indicate independent repeats of the experiment. Statistical significance (***$P$ < 0.001) was
999 revealed by Student's *t*-test. Expression of RFP-AIMp was verified at 6 dpi with an anti-RFP
1000 blot (inset).
1001
1002 **Figure 2: Xanthomonas T3E XopL is suppressing autophagy**
1003 **(A)** RLUC-ATG8a or RLUC-NBR1 constructs were coexpressed with internal control FLUC
1004 in *N. benthamiana*. XopL or GFP constructs were co-infiltrated. RLUC and FLUC signals were
1005 simultaneously measured in leaf extracts at 48 h post- infiltration using the dual-luciferase
1006 system. Values represent the ratio of RLUC-ATG8a and FLUC activities to the mean of control
1007 (n=4Statistical significance ($P$ < 0.01) was shown by Student's *t*-test. The experiment was
1008 repeated more than 3 times by with similar results.
1009 **(B)** Immunoblot analysis of NBR1 and ATG8 protein levels in *N. benthamiana* plants
1010 transiently expressing GFP-XopL or GFP control at 2dpi verified with an anti-GFP antibody.
1011 Ponceau Staining (PS) served as a loading control. The experiment was repeated at least three
1012 times with similar results.
1013 **(C)** Immunoblot analysis of NBR1 and ATG8 protein levels in *N. benthamiana* plants
1014 transiently expressing XopL or GUS control at 2dpi after ConA or DMSO treatment.
1015 Expression of GFP-XopL was verified with an anti-GFP antibody, while expression of GUS-
1016 HA was confirmed with an anti-HA antibody. Ponceau Staining (PS) served as a loading
1017 control. The experiment was repeated twice with similar results.
1018 **(D)** GFP-ATG8g-labeled autophagosomes were quantified from plants infected with *Xcv*
1019 *ΔxopQ* or *Xcv ΔxopQ ΔxopL* at 2 dpi in the presence or absence of ConA. Puncta were calculated
1020 from z-stacks (15) of $n$=12 individuals using ImageJ. Statistical significance (** $P$ < 0.01, ***
1021 $P$ < 0.001) was determined by one way ANOVA. The experiment was repeated twice with
1022 similar results.
1023 **(E)** Immunoblot analysis of NBR1 and ATG8 protein levels in Xcv *ΔxopQ,* Xcv *ΔxopQ ΔxopL*
1024 or mock infected *N. benthamiana* plants at 2dpi. Ponceau Staining (PS) served as a loading
1025 control. The experiment was repeated twice with similar results.
1026 **(F)** RLUC-ATG8a or RLUC-NBR1 constructs were coexpressed with internal control FLUC
1027 in *N. benthamiana*. *Xcv ΔxopQ and Xcv ΔxopQ ΔxopL* were co-infiltrated with Agrobacteria
1028 containing the respective constructs. RLUC and FLUC activities were simultaneously measured

1029 in leaf extracts at 48 h post- infiltration using the dual-luciferase system. Values represent the
1030 ratio of RLUC-ATG8a and FLUC activities and error bars show SD (n=4). Statistical
1031 significance comparing *Xcv ΔxopQ and Xcv ΔxopQ ΔxopL* values (***$P < 0.001$) was revealed
1032 by Student's *t*-test. The experiment was repeated 3 times with similar results.
1033
1034 **Figure 3: XopL interacts with and degrades SH3P2 and to boost *Xcv* virulence**
1035 **(A)** Interaction of XopL with SH3P2 in yeast two-hybrid assays. XopL fused to the GAL4
1036 DNA-binding domain was expressed in combination with SH3P2 fused to the GAL4 activation
1037 domain (AD) in yeast strain Y190. Cells were grown on selective media before a LacZ filter
1038 assay was performed. pSV40/p53 served as positive control, while the empty AD or BD vector
1039 served as negative control. NtSH3P2 = *Nicotiana tabacum* SH3P2. –LT = yeast growth on
1040 medium without Leu and Trp, –HLT = yeast growth on medium lacking His, Leu, and Trp,
1041 indicating expression of the HIS3 reporter gene. LacZ, activity of the lacZ reporter gene.
1042 **(B)** Coimmunoprecipitation of GFP-XopL with AtSH3P2-HA. GFP-XopL or GFP were
1043 transiently coexpressed with AtSH3P2-HA in leaves of *N. benthamiana*. After 48 h, total
1044 proteins (Input) were subjected to immunoprecipitation (IP) with GFP-Trap beads, followed by
1045 immunoblot analysis using either anti-GFP or anti-HA antibodies. AtSH3P2 = *Arabidopsis*
1046 *thaliana* SH3P2. Two repetitions with similar results have been conducted.
1047 **(C)** Visualization of protein interactions *in planta* by the bimolecular fluorescence
1048 complementation assay. Yellow fluorescent protein (YFP) confocal microscopy images show
1049 *Nicotiana benthamiana* leaf epidermal cells transiently expressing $Venus^{N173}$-XopL in
1050 combination with AtSH3P2-$Venus^{C155}$. A positive control showing the dimerization of
1051 fructose-1,6-bisphosphatase (FBPase) within the cytosol. The red structures indicate
1052 autofluorescence of chloroplasts. The combination of $Venus^{N173}$-XopL with FBPase-$Venus^{C155}$
1053 or $Venus^{N173}$-FBPase with AtSH3P2-$Venus^{C155}$ do not induce YFP fluorescence and serve as
1054 negative controls. Bars = 20 µm.
1055 **(D)** Colocalization analysis of GFP-XopL with SH3P2-RFP, RFP-ATG8e and RFP-ATG8g in
1056 *N. benthamiana* leaves. Imaging was performed 2 d after transient expression and images
1057 represent single confocal planes from abaxial epidermal cells (scale bars = 20 µm and 10 µm,
1058 lower panel). White arrows indicate colocalization of GFP and RFP signals. The experiment
1059 was repeated twice with similar results.
1060 **(E)** Total proteins were extracted 48 hpi with *A. tumefaciens* harboring the respective GFP-
1061 XopL, HA-XopL and SH3P2-GFP expression constructs. SH3P2-GFP protein levels (lower
1062 band) were detected using an anti-GFP antibody. Expression of the XopL was verified using an
1063 anti-HA or anti-GFP antibody. Expression of GUS-HA served as a control. Ponceau S staining
1064 serves as a loading control. The experiment was repeated three times with similar results.
1065 **(F)** Growth of Xcv *and* Xcv *ΔxopL* strains in *roq1 N. benthamiana* plants silenced for SH3P2
1066 (pTRV2-*SH3P2*) compared to control plants (pTRV2). Leaves were dip-inoculated with a
1067 bacteria suspension at $OD_{600} = 0.2$ and bacteria were quantified at 3 and 6 dpi. Red and yellow
1068 data points indicate experimental repeats. Different letters indicate statistically significant
1069 differences ($P < 0.05$) as determined by one-way ANOVA.
1070
1071 **Figure 4. XopL mediates the proteasome degradation of SH3P2 via its E3 ligase activity**
1072 **(A)** SH3P2-GFP was transiently coexpressed together with GUS-HA and GFP-XopL in *N.*
1073 *benthamiana* using agroinfiltration. At 42 hpi, 200 µM MG132 was infiltrated into *A.*
1074 *tumefaciens*-inoculated leaves, and leaf material was collected 48 hpi. Expression of SH3P2-
1075 GFP (lower band) and GFP-XopL (upper band) was detected using an anti-GFP antibody. GUS-
1076 HA expression was confirmed with an anti-HA antibody. Ponceau S staining serves as a loading
1077 control. The experiment was repeated three times with similar results.
1078 **(B)** *In vitro* ubiquitination assay reveals ubiquitination of SH3P2 by XopL. GST-XopL, and
1079 MBP-SH3P2 were tested using the Arabidopsis His-AtUBA1 and His-AtUBC8. Lanes 2 to 4

are negative controls. Proteins were separated by SDS-PAGE and detected by immunoblotting using the indicated antibodies. The experiment was repeated twice with similar results.
**(C)** SH3P2-GFP was transiently coexpressed together with GFP, GFP-XopL and GFP-XopL ΔE3 in *N. benthamiana* using agroinfiltration. GFP protein levels were detected with an anti-GFP antibody. Ponceau S staining serves as a loading control. The experiment was repeated three times with similar results.
**(D)** Immunoblot analysis of ATG8 protein levels in *N. benthamiana* plants transiently expressing GFP-XopL, GFP-XopL ΔE3 or GFP control at 2dpi. Expression of binary constructs was verified with an anti-GFP antibody. Ponceau Staining (PS) served as a loading control. The experiment was repeated twice with similar results.
**(E)** RLUC-ATG8a constructs were coexpressed with internal control FLUC in *N. benthamiana*. GFP-XopL, GFP-XopL ΔE3 or GFP control were co-infiltrated together with RLUC/FLUC mixture. *Renilla* and *Firefly* luciferase activities were simultaneously measured in leaf extracts at 48 hpi using the dual-luciferase system. Values represent the ratio of RLUC-ATG8a and FLUC activities (n=4). Statistical significance (* $P < 0.5$, ** $P < 0.01$) was revealed by Student's *t*-test. The experiment was repeated 3 times. Expression of proteins was verified with indicated antibodies.

**Figure 5: XopL is ubiquitinated in planta and degraded by NBR1-mediated selective autophagy**
**(A)** GFP-XopL was coexpressed with GFP or AIMp-RFP. Proteins were separated by SDS-PAGE and detected by immunoblotting using the indicated antibodies. Ponceau Staining (PS) served as a loading control. The experiment was repeated three times with similar results.
**(B)** Colocalization of GFP-XopL with RFP-Joka2 in *N. benthamiana* leaves. Imaging was performed 2 d after transient expression and images represent single confocal planes from abaxial epidermal cells (bars = 20 µm). The experiment was repeated twice with similar results.
**(C)** FRET FLIM measurements of GFP-Joka2 and RFP-XopL in *N. benthamiana* leaves. The freeRFP construct served as a negative control and RFP-ATG8E (n = 9) as a positive control. Scattered points show individual data points, color indicates biological repeats. The lifetime (in ns) of GFP-Joka2 (donor, n = 41) was significantly reduced in the presence of RFP-XopL (n = 40) but not in the presence of freeRFP (n = 35). Significant differences were calculated using Wilcoxon rank sum test, with significantly different groups denoted by different letters. The experiment was repeated three times with similar results.
**(D)** Immunoprecipitation (IP) of GFP-XopL reveals association with NBR1. Immunoblots of input and IP samples from *N. benthamiana* plants transiently expressing GFP or GFP-XopL were probed with anti-GFP and anti-NBR1 antibodies.
**(E)** Immunoprecipitation (IP) of GFP-XopL and GFP-XopL ΔE3 reveals association with NBR1. Immunoblots of input and IP samples from *N. benthamiana* plants transiently expressing GFP, GFP-XopL and GFP-XopL ΔE3 were probed with anti-GFP and anti-NBR1 antibodies.
**(F)** GFP-XopL was transiently expressed in pTRV2, pTRV2-Joka2 and *N. benthamiana* WT plants. Expression of binary constructs was verified with an anti-GFP antibody. Joka2 silencing was verified using an anti-NBR1 antibody. Ponceau Staining (PS) served as a loading control. The experiment was repeated twice with similar results.
**(G)** Growth of Xcv *ΔxopQ* in *N. benthamiana* plants silenced for *Joka2* (pTRV2-Joka2) compared to control plants (pTRV2). Leaves were dip-inoculated with a bacteria suspension at $OD_{600}$ = 0.2. and bacteria were quantified at 3 and 6 dpi. Red, blue, and green data points represent repeats of the experiments. Significant differences were calculated using Student's *t-test* and are indicated by: **, $P < 0.01$. The experiment was repeated three times with similar trends.

1130 **(H)** GFP-XopL, GFP-XopL ΔE3 were transiently expressed in *N. benthamiana*. AIMp-RFP
1131 was co-infiltrated to stabilize both XopL variants. Samples were taken 48 hpi, and total proteins
1132 (Input) were subjected to immunoprecipitation (IP) with GFP-Trap beads, followed by
1133 immunoblot analysis of the precipitates using either anti-GFP or anti-ubiquitin antibodies. GFP
1134 served as a negative control. RFP-AIMp expression was verified by an anti-RFP antibody. The
1135 experiment was repeated three times with similar results.
1136 **(I)** GFP-XopL was transiently expressed in *N. benthamiana*. Samples were taken 48 hpi, and
1137 total proteins (Input) were subjected to immunoprecipitation (IP) with the ubiquitin pan
1138 selector, followed by immunoblot analysis of the precipitates using either anti-GFP or anti-
1139 ubiquitin antibodies. GFP served as a control. Asterisk indicates the GFP-XopL full-length
1140 protein. The experiment was repeated two times with similar results.
1141 **(J)** Immunoblot analysis GFP-XopL and GFP-XopL$_{K191A}$ at 1 and 2 dpi using an anti-GFP
1142 antibody. Ponceau Staining (PS) served as a loading control. The experiment was repeated three
1143 times with similar results.
1144 **(K)** GFP-XopL and GFP-XopL$_{K191A}$ were transiently expressed in *N. benthamiana*. Samples
1145 were taken 48 hpi, and total proteins (Input) were subjected to immunoprecipitation (IP) with
1146 GFP-Trap beads, followed by immunoblot analysis of the precipitates using either anti-GFP,
1147 anti-ubiquitin and anti-NBR1 antibodies. GFP served as a control. The experiment was repeated
1148 three times with similar results.
1149
1150 **Figure 6: Model illustrating the function of XopL**
1151 **(A) Xenophagy of XopL:** Upon delivery of XopL in the plant XopL undergoes self-
1152 ubiquitination and possible ubiquitination by an unknown host E3 ligase. Joka2/NBR1
1153 associates with XopL and triggers its degradation via the selective autophagy pathway in the
1154 vacuole. **(B) XopL blocks autophagy**: XopL interacts with autophagy component SH3P2
1155 inside the cell and ubiquitinates it to degrade it via the 26S proteasome. Degradation of SH3P2
1156 results in defects of autophagosome delivery into the vacuole and hence suppresses autophagy.
1157
1158 **Fig. S1: Silencing of *ATG7* in *N. benthamiana* plants abolishes autophagosome formation**
1159 **and Xcv blocks autophagy at 6hpi.**GFP-ATG8e-labeled puncta were quantified from plants
1160 silenced for *ATG7* (pTRV2-ATG7) infected with mock or Xcv *ΔxopQ* at 6hpi in the presence
1161 or absence of ConA, and of AZD. Puncta were calculated from z-stacks (X) of $n$=12 individuals
1162 using ImageJ. Different letters indicate statistically significant different groups ($P < 0.05$) as
1163 determined by one way ANOVA.
1164 **(B)** RLUC-ATG8a or RLUC-NBR1 constructs were coexpressed with internal control FLUC
1165 in *N. benthamiana*. *Xcv ΔxopQ* or infiltration buffer (mock) was co-infiltrated with
1166 Agrobacteria containing the respective constructs. RLUC and FLUC activities were
1167 simultaneously measured in leaf extracts at 8 h post- infiltration using the dual-luciferase
1168 system. Values represent the mean ratio of RLUC-ATG8a and FLUC activities (n=4).
1169 Statistical significance (***$P < 0.001$) was revealed by Student's *t*-test. The experiment was
1170 repeated 3 times with similar results.
1171
1172 **Fig. S2: Virus induced gene silencing of *ATG7* in *N. benthamiana* is beneficial for Xcv.**
1173 **(A)** Growth of Xcv *ΔxopQ* in *N. benthamiana* plants silenced for *ATG7* (pTRV2-*ATG7*)
1174 compared to control plants (pTRV2). Leaves were dip-inoculated with a bacteria suspension at
1175 $OD_{600}$ = 0.2 and bacteria were quantified at 6 dpi. Data represent the mean SD (n = 6).
1176 Significant differences were calculated using Student's *t-test* and are indicated by **, $P < 0.01$.
1177 The experiment was repeated twice with similar trends. Red and yellow data points represent
1178 repeats of the experiment.

1179 **(B)** qRT-PCR analysis of *ATG7* mRNA levels in silenced *N. benthamiana* plants. *Actin*
1180 expression was used to normalize the expression value in each sample, and relative expression
1181 values were determined against the mean expression in pTRV2 (control) plants**.**
1182
1183 **Fig. S3: Suppression of autophagy is enhanced by T3Es.**
1184 **(A)** Immunoblot analysis of NBR1 and ATG8 protein levels in Xcv *ΔxopQ, ΔhrcN* or mock
1185 infected *N. benthamiana* plants at 1 and 2dpi. Ponceau Staining (PS) served as a loading control.
1186 The experiment was repeated twice with similar results.
1187 **(B)** Autophagic flux determined by quantitative dual-luciferase assay. RLUC-ATG8a or
1188 RLUC-NBR1 constructs were coexpressed with internal control FLUC in *N. benthamiana*. Xcv
1189 *ΔxopQ* and *ΔhrcN* were respectively co-infiltrated with Agrobacteria containing the luciferase
1190 constructs. Renilla and Firefly luciferase activities were simultaneously measured in leaf
1191 extracts at 48 h post- infiltration using the dual-luciferase system. Values represent the ratio of
1192 RLUC-ATG8a and FLUC activities normalized to mock (n=4). Statistical significance
1193 (**$P$<0.01) was revealed by Student's *t*-test. The experiment was repeated 2 times with similar
1194 results.
1195 **(C)** RT-qPCR analysis of *NbATG8-1.1/1.2* and *NbJoka2* transcript levels upon challenge of *N.*
1196 *benthamiana* plants with Xcv *ΔxopQ* and *ΔhrcN* for 1 and 2 dpi compared to mock infected
1197 plants. Values represent expression relative to mock control of respective time point and were
1198 normalized to *actin*. Statistical significance (*** $P < 0.001$) was revealed by Student's *t*-test.
1199
1200 **Fig. S4: Screening for Xanthomonas T3Es with altered autophagic flux.**
1201 **(A)** RLUC-ATG8a constructs were coexpressed with internal control FLUC in *N. benthamiana*.
1202 GFP-XopL, XopJ-GFP, XopD-GFP and XopS-HA were co-infiltrated with Agrobacteria
1203 carrying the RLUC-ATG8a and FLUC constructs. Renilla and Firefly luciferase activities were
1204 simultaneously measured in leaf extracts at 48 h post- infiltration using the dual-luciferase
1205 system. Values represent the ratio of RLUC-ATG8a to FLUC activity normalized to GFP
1206 control (XopL, XopJ, XopD, AIMp; n=20; XopS n=4). Expression of T3Es and RFP-AIMp
1207 were verified with the indicated antibodies.
1208 **(B)** RLUC-ATG8a constructs were coexpressed with internal control FLUC in *N. benthamiana*.
1209 Plants were treated with MG132 for 6 hours prior measurement. Values represent the ratio of
1210 RLUC-ATG8a to FLUC activity normalized to vector control (n=8). Statistical significance (*
1211 $P < 0.5$) was revealed by Student's *t*-test.
1212 **(C)** RT-qPCR analysis of *NbATG8-2.1/2.2* and *NbJoka2* transcript levels upon Agrobacteria-
1213 mediated transient expression of GFP, GFP-XopL or AIMp for 1 and 2 dpi. Values represent
1214 expression relative to GFP control of respective time point and were normalized to *actin*.
1215 Statistical significantly different groups are denoted by different letters, as calculated using
1216 Kruskal-Wallis rank sum test ($P$<0.05).
1217
1218 **Fig. S5: XopL contributes to Xcv virulence.**
1219 **(A)** Growth of Xcv 85-10 (vector) (white bar), Xcv 85-10 Δ*xopL* (vector) (grey bar), and Xcv
1220 85-10 Δ*xopL* (*xopL*) (black bar) strains in tomato VF36 leaves. Leaves were dipped in a 2 x $10^8$
1221 CFU/mL suspension of bacteria. The number of bacteria in each leaf was quantified at 10 dpi.
1222 Data points represent mean $\log_{10}$ colony-forming units per $cm^2$ ± SD of three plants. Different
1223 letters above bars indicate statistically significant (Tukey's honestly significant difference
1224 (HSD) test, P < 0.05) differences between samples. Vector = pBBR1MCS-2.
1225 **(B)** Delayed disease symptom development in tomato leaves inoculated with *Xcv* or *Xcv* Δ*xopL*.
1226 Tomato leaves inoculated with strains described in (A) were photographed at 14 dpi.
1227 **(C)** Growth of Xcv 85-10, Xcv 85-10 Δ*xopL* strains in *roq1 N. benthamiana* leaves. Leaves
1228 were dipped in a 2 x $10^8$ CFU/mL suspension of bacteria. The number of bacteria in each leaf

was quantified at 10 dpi (n = 5). Significant differences were calculated using Student's *t-test* (**, P < 0.01). The experiment was repeated twice with similar trends.
**(D)** Delayed disease symptom development in *roq1 N. benthamiana* leaves dip-inoculated with *Xcv* or *Xcv* Δ*xopL*. *N. benthamiana roq1* leaves inoculated with strains described in (C) were photographed at 10 dpi.
**(E)** Delayed symptom development in *roq1 N. benthamiana* leaves inoculated with *Xcv* or *Xcv* Δ*xopL*. Leaves were syringe-inoculated with $OD_{600}$=0.2 and photographed at 3 dpi.

**Fig. S6: Joka2 bodies are induced during Xcv infection in a XopL-dependent manner.**
**(A)** GFP-ATG8e-labeled autophagosomes imaged from *N. benthamiana* plants infected with mock, Xcv or *Xcv* Δ*xopL* at 2 dpi in the presence or absence of ConA (bars = 10 µm).
**(B)** Joka2-RFP labelled puncta or aggregates upon challenge of *N. benthamiana* leaves with mock, *Xcv* or *Xcv* Δ*xopL* infection at 1dpi.

**Fig. S7: Transgenic *A. thaliana* GFP-XopL plants display defects in autophagic degradation**
**(A)** Immunoblot analysis of NBR1 protein levels in transgenic UBQ::GFP-XopL plants or Col-0. Plants were treated with concanamycin A (ConA) for 6 hours. Expression of GFP-XopL was verified with an anti-GFP antibody. Ponceau S staining serves as a loading control.
**(B)** 5 weeks old *A. thaliana* plants expressing UBQ::GFP-XopL develop an early senescence phenotype reminiscent of autophagy deficient mutants.
**(C)** Localization analysis of GFP-XopL of transgenic *A. thaliana* UBQ::GFP-XopL #23 line. Image represents single confocal planes from abaxial epidermal cells (bars = 5 µm).
**(D)** RT-qPCR analysis of *ATG8a* and *NBR1* transcript levels in *Arabidopsis thaliana* GFP or GFP-XopL plants. Values represent expression (n=3) relative to GFP control and were normalized to *PP2A*. Statistical significance (**P*<0.05) was revealed by Student's *t*-test.

**Fig. S8: SH3P2 is conserved in different plant species.**
**(A)** Protein sequence alignment of SH3P2 from different species. The alignment was generated using CLUSTALW2 with default parameters and BoxShade 3.21. Positions of identical and similar sequences are boxed in black and grey, respectively. The following sequences were used to build the alignment: *Arabidopsis thaliana*, *Nicotiana tabacum, Nicotiana benthamiana*, *Solanum lycopersicum*.
**(B)** Phylogentic analysis of the SH3P2 from different plant species.
**(C)** XopL interacts with SH3P2 from *Nicotiana tabacum* and *Nicotiana benthamiana*. Interaction of XopL with SH3P2 in yeast two-hybrid assays. XopL fused to the GAL4 DNA-binding domain was expressed in combination with SH3P2 fused to the GAL4 activation domain (AD) in yeast strain Y190. Cells were grown on selective media before a LacZ filter assay was performed. The empty AD or BD vector served as negative control. NtSH3P2 = *Nicotiana tabacum* SH3P2, NbSH3P2 = *Nicotiana benthamiana* –LT = yeast growth on medium without Leu and Trp, –HLT = yeast growth on medium lacking His, Leu, and Trp, indicating expression of the HIS3 reporter gene. LacZ, activity of the lacZ reporter gene.
**(D)** *In vitro* co-IP assay showing direct interaction of XopL with AtSH3P2. MBP-XopL and GST-AtSH3P2 were expressed in E. coli. Pull down was performed using amylose resin. Proteins were detected in an immunoblot using antibodies as indicated.

**Supp Video 1: XopL/SH3P2 puncta are mobile**
*Nicotiana benthamiana* leaf epidermal cells transiently expressing $Venus^{N173}$-XopL in combination with AtSH3P2-$Venus^{C155}$.

1279 **Fig. S9: Silencing of SH3P2 in *N. benthamiana* perturbs autophagy.**
1280 **(A)** qRT-PCR analysis of SH3P2 mRNA levels in silenced plants. *Actin* expression was used
1281 to normalize the expression value in each sample, and relative expression values were
1282 determined against pTRV2 control plants (set to 1).
1283 **(B)** Phenotype of SH3P2-VIGS plants in comparison to the pTRV2 control. Picture was taken
1284 14 dpi.
1285 **(C)** Immunoblot analysis of ATG8 protein levels in *N. benthamiana* pTRV2 (control) and
1286 pTRV2-*SH3P2* (*SH3P2* silencing) 2 weeks after VIGS. Ponceau Staining (PS) served as a
1287 loading control. The experiment was repeated twice with similar results.
1288 **(D)** GFP-ATG8e-labeled autophagosomes were quantified from pTRV2 or pTRV2-SH3P2
1289 plants transiently expressing GFP-ATG8e at 2dpi in the presence of autophagy inducer AZD =
1290 AZD8055 and AZD/ConA. Puncta were calculated from z-stacks of $n$=10 individuals using
1291 ImageJ. Statistical significance (*** $P < 0.5$) was revealed by Student's $t$-test comparing
1292 number of autophagosomes in AZD/ConA treatments in pTRV2 and pTRV2-*SH3P2* plants.
1293 The experiment was repeated twice with similar results.
1294
1295 **Fig. S10: Gene expression of SH3P2 is induced by XopL and XopL-mediated degradation**
1296 **is due to post-transcriptional degradation events.**
1297 qRT-PCR analysis of AtSH3P2-specific mRNA levels in *N. benthamiana* plants transiently
1298 expressing AtSH3P2-HA, upon coexpression with GFP or GFP-XopL. *Actin* expression was
1299 used to normalize the expression value in each sample. Values represent *AtSH3P2* transcript
1300 level normalized to control (n=4).
1301
1302 **Fig. S11: RFP-XopL ΔE3 co-localizes with and is unable to ubiquitinate SH3P2-GFP.**
1303 **(A)** Colocalization analysis of RFP-XopL ΔE3 with SH3P2-GFP in *N. benthamiana* leaves.
1304 Imaging was performed 2 d after transient expression and images represent single confocal
1305 planes from abaxial epidermal cells (bars = 20 μm).
1306 **(B)** *In vitro* ubiquitination assay reveals GST-XopL ΔE3 is unable to ubiquitinate MBP-SH3P2.
1307 GST-XopL, ΔE3 and MBP-SH3P2 were tested using the Arabidopsis His-AtUBA1 and His-
1308 AtUBC8. Lanes 2 to 4 are negative controls, while Lane 5 is the positive control with GST-
1309 XopL. Proteins were separated by SDS-PAGE and detected by immunoblotting using the
1310 indicated antibodies. The experiment was repeated three times with similar results.
1311
1312 **Fig. S12 XopL is degraded in the vacuole**. Localization of GFP-XopL in the presence or
1313 absence of ConA in transgenic GFP-XopL. DMSO or 0.5 μM ConA was used to treat seedlings,
1314 followed by confocal imaging of the roots. GFP-labeled puncta detectable upon ConA treatment
1315 indicate XopL accumulation in the vacuole (bars = 20 μm).
1316
1317 **Fig. S13: Virus-induced gene silencing of *Joka2* in *N. benthamiana* plants.**
1318 **(A)** qRT-PCR analysis of Joka2 mRNA levels in *Joka2* silenced pepper plants. *Actin* expression
1319 was used to normalize the expression value in each sample, and relative expression values were
1320 determined against pTRV2 control plants (set to 1)**.**
1321 **(B)** Immunoblot analysis of GFP and GFP-XopL protein levels in *N. benthamiana* plants
1322 silenced for *Joka2* (pTRV2-Joka2) compared against control (pTRV2). Ponceau staining (PS)
1323 served as a loading control.
1324
1325 **Fig. S14: XopL in planta ubiquitination is enhanced by the presence of AIMp** GFP-XopL
1326 or GFP were transiently expressed in *N. benthamiana*. RFP-AIMp was co-infiltrated. Samples
1327 were taken 48 hpi, and total proteins (Input) were subjected to immunoprecipitation (IP) with
1328 the ubiquitin pan selector, followed by immunoblot analysis of the precipitates using either anti-
1329 GFP or anti-ubiquitin antibodies. RFP-AIMp expression was verified by an anti-RFP antibody.

1330 Asterisk indicates the GFP-XopL full-length protein. The experiment was repeated twice with
1331 similar results.
1332
1333 **Fig. S15: XopL is ubiquitinated *in planta* and undergoes self-ubiquitination**
1334 **(A)** XopL ubiquitination site at lysine 191 was identified in vivo by LC-MS/MS. GFP-XopL
1335 was transiently expressed in *N. benthamiana* and total proteins were subjected to anti-GFP IP
1336 followed by trypsin digestion. Ubiquitinated peptides were detected by LC-MS/MS. The
1337 spectrum shows the fragmentation pattern of the GlyGly modified peptide
1338 ALglKATADLLEDATQPGR corresponding to amino acids 189-205.
1339 **(B)** *In vitro* ubiquitination assay reveals autoubiquitination of XopL. Ubiquitination of MBP-
1340 XopL was tested using the Arabidopsis His-AtUBA1 and His-AtUBC8. Lanes 2 to 4 are
1341 negative controls. Proteins were separated by SDS-PAGE and detected by immunoblotting
1342 using the indicated antibodies. Arrows in the MBP blot indicate higher molecular weight bands
1343 of MBP-XopL and autoubiquitination events. The experiment was repeated twice with similar
1344 results.
1345 **(C)** XopL ubiquitination site at lysine 191 was identified in vitro by LC-MS/MS. GST-XopL
1346 was used in an in vitro ubiquitination assay and samples were subjected to trypsin digestion.
1347 Ubiquitinated peptides were detected by LC-MS/MS. The spectrum shows the fragmentation
1348 pattern of the GlyGly modified peptide ALglKATADLLEDATQPGR corresponding to amino
1349 acids 189-205.
1350
1351 **Fig. S16: C Characterization of XopLK191A variant in vitro and in planta.**
1352 **(A)** *In vitro* ubiquitination assay reveals less autoubiquitination of XopL K191A compared to
1353 XopL WT. Ubiquitination of GST-XopL was tested using the Arabidopsis His-AtUBA1 and
1354 His-AtUBC8. Lanes 3 to 5 are negative controls. Proteins were separated by SDS-PAGE and
1355 detected by immunoblotting using the indicated antibodies. The experiment was repeated twice
1356 with similar results.
1357 **(B)** Localization analysis of GFP-XopL$_{K191A}$ in *N. benthamiana* leaves. Imaging was performed
1358 2 d after transient expression and images represent single confocal planes from abaxial
1359 epidermal cells (bars = 20 μm).
1360 **(C)** qRT-PCR analysis of GFP-XopL and GFP-XopL K191A mRNA levels in *N. benthamiana*
1361 plants during transient expression. *Actin* expression was used to normalize the expression value
1362 in each sample.
1363 **(D)** GFP-XopL and GFP-XopL$_{K191A}$ were transiently expressed in *N. benthamiana*. RFP-AIMp
1364 was co-infiltrated. Samples were taken 48 hpi, and total proteins (Input) were subjected to
1365 immunoprecipitation (IP) with the ubiquitin pan selector, followed by immunoblot analysis of
1366 the precipitates using either anti-GFP or anti-ubiquitin antibodies. GFP served as a control.
1367 RFP-AIMp expression was verified by an anti-RFP antibody. Asterisk indicates the GFP-XopL
1368 full-length protein. The experiment was repeated twice with similar results.
1369
1370 **Fig. S17: XopL ΔE3 is degraded by autophagy.**
1371 **(A)** GFP, GFP-XopL, or GFP-XopL ΔE3 was coexpressed with RFP-AIMp or RFP control in
1372 *N. benthamiana*. Samples were taken at 2 dpi, total proteins extracted and immunoblotted using
1373 the indicated antibodies. Ponceau Staining (PS) served as a loading control.
1374 **(B)** Immunoblot of transiently expressed GFP-XopL ΔE3 in *N. benthamiana* after treatment of
1375 ConA or DMSO carrier. Ponceau Staining (PS) served as a loading control.
1376
1377 **Fig. S18: XopL K191 residue is highly conserved through the Xanthomonas genus**
1378 **(A)** Sequence alignment of XopL protein from *Xcv* with related effectors from *Xanthomonas*
1379 genus or more distantly related plant pathogen bacteria. Colors represent amino acid
1380 conservation through the alignment, with red for highly conserved residues, blue for lower

conservation and grey for no conservation. Identical amino acid percentage to XopL$^{Xcv}$ is displayed to the right of the alignment.
**(B)** Closer view of the region 201-299 of the alignment with amino acids colored according to the Rasmol coloration. Lysine K191 is indicated with a red arrow.

## References


Adams EHG, Spoel SH (2018) The ubiquitin-proteasome system as a transcriptional regulator of plant immunity. *J Exp Bot* 69: 4529-4537

Adlung N, Prochaska H, Thieme S, Banik A, Bluher D, John P, Nagel O, Schulze S, Gantner J, Delker C *et al* (2016) Non-host Resistance Induced by the *Xanthomonas* Effector XopQ Is Widespread within the Genus Nicotiana and Functionally Depends on EDS1. *Front Plant Sci* 7: 1796

Ahn G, Kim H, Kim DH, Hanh H, Yoon Y, Singaram I, Wijesinghe KJ, Johnson KA, Zhuang X, Liang Z *et al* (2017) SH3 Domain-Containing Protein 2 Plays a Crucial Role at the Step of Membrane Tubulation during Cell Plate Formation. *Plant Cell* 29: 1388-1405

Albers P, Üstün S, Witzel K, Kraner M, Börnke F (2019) A Remorin from *Nicotiana benthamiana* Interacts with the *Pseudomonas* Type-III Effector Protein HopZ1a and is Phosphorylated by the Immune-Related Kinase PBS1. *Mol Plant Microbe Interact* 32: 1229-1242

Banfield MJ (2015) Perturbation of host ubiquitin systems by plant pathogen/pest effector proteins. *Cell Microbiol* 17: 18-25

Borchert N, Dieterich C, Krug K, Schutz W, Jung S, Nordheim A, Sommer RJ, Macek B (2010) Proteogenomics of Pristionchus pacificus reveals distinct proteome structure of nematode models. *Genome Res* 20: 837-846

Büttner D (2016) Behind the lines-actions of bacterial type III effector proteins in plant cells. *FEMS Microbiol Rev* 40: 894-937

Chai Q, Wang X, Qiang L, Zhang Y, Ge P, Lu Z, Zhong Y, Li B, Wang J, Zhang L *et al* (2019) A *Mycobacterium tuberculosis* surface protein recruits ubiquitin to trigger host xenophagy. *Nat Commun* 10: 1973

Clough SJ, Bent AF (1998) Floral dip: a simplified method for Agrobacterium-mediated transformation of *Arabidopsis thaliana*. *Plant J* 16: 735-743

Dagdas YF, Belhaj K, Maqbool A, Chaparro-Garcia A, Pandey P, Petre B, Tabassum N, Cruz-Mireles N, Hughes RK, Sklenar J *et al* (2016) An effector of the Irish potato famine pathogen antagonizes a host autophagy cargo receptor. *Elife* 5

Dagdas YF, Pandey P, Tumtas Y, Sanguankiattichai N, Belhaj K, Duggan C, Leary AY, Segretin ME, Contreras MP, Savage Z *et al* (2018) Host autophagy machinery is diverted to the pathogen interface to mediate focal defense responses against the Irish potato famine pathogen. *Elife* 7

Dauphinee AN, Cardoso C, Dalman K, Ohlsson JA, Fick SB, Robert S, Hicks GR, Bozhkov PV, Minina EA (2019) Chemical Screening Pipeline for Identification of Specific Plant Autophagy Modulators. *Plant Physiol* 181: 855-866

Dupont N, Lacas-Gervais S, Bertout J, Paz I, Freche B, Van Nhieu GT, van der Goot FG, Sansonetti PJ, Lafont F (2009) Shigella phagocytic vacuolar membrane remnants participate in the cellular response to pathogen invasion and are regulated by autophagy. *Cell Host Microbe* 6: 137-149

Erickson JL, Adlung N, Lampe C, Bonas U, Schattat MH (2018) The *Xanthomonas* effector XopL uncovers the role of microtubules in stromule extension and dynamics in *Nicotiana benthamiana*. *Plant J* 93: 856-870

Furlan G, Klinkenberg J, Trujillo M (2012) Regulation of plant immune receptors by ubiquitination. *Front Plant Sci* 3: 238

Furlan G, Nakagami H, Eschen-Lippold L, Jiang X, Majovsky P, Kowarschik K, Hoehenwarter W, Lee J, Trujillo M (2017) Changes in PUB22 Ubiquitination Modes Triggered by MITOGEN-ACTIVATED PROTEIN KINASE3 Dampen the Immune Response. *Plant Cell* 29: 726-745

Gantner J, Ordon J, Kretschmer C, Guerois R, Stuttmann J (2019) An EDS1-SAG101 Complex Is Essential for TNL-Mediated Immunity in *Nicotiana benthamiana*. *Plant Cell* 31: 2456-2474

Germic N, Frangez Z, Yousefi S, Simon HU (2019) Regulation of the innate immune system by autophagy: neutrophils, eosinophils, mast cells, NK cells. *Cell Death Differ* 26: 703-714

Gomes LC, Dikic I (2014) Autophagy in antimicrobial immunity. *Mol Cell* 54: 224-233

Grefen C, Donald N, Hashimoto K, Kudla J, Schumacher K, Blatt MR (2010) A ubiquitin-10 promoter-based vector set for fluorescent protein tagging facilitates temporal stability and native protein distribution in transient and stable expression studies. *Plant J* 64: 355-365

Gu Y, Zavaliev R, Dong X (2017) Membrane Trafficking in Plant Immunity. *Mol Plant* 10: 1026-1034

Hafrén A, Macia JL, Love AJ, Milner JJ, Drucker M, Hofius D (2017) Selective autophagy limits cauliflower mosaic virus infection by NBR1-mediated targeting of viral capsid protein and particles. *Proc Natl Acad Sci U S A* 114: E2026-E2035

Hafrén A, Üstün S, Hochmuth A, Svenning S, Johansen T, Hofius D (2018) Turnip Mosaic Virus Counteracts Selective Autophagy of the Viral Silencing Suppressor HCpro. *Plant Physiol* 176: 649-662

Hu H, Sun SC (2016) Ubiquitin signaling in immune responses. *Cell Res* 26: 457-483

Huang J, Brumell JH (2014) Bacteria-autophagy interplay: a battle for survival. *Nat Rev Microbiol* 12: 101-114

Khan M, Seto D, Subramaniam R, Desveaux D (2018) Oh, the places they'll go! A survey of phytopathogen effectors and their host targets. *Plant J* 93: 651-663

Kim JG, Stork W, Mudgett MB (2013) *Xanthomonas* type III effector XopD desumoylates tomato transcription factor SlERF4 to suppress ethylene responses and promote pathogen growth. *Cell Host Microbe* 13: 143-154

Kim JG, Taylor KW, Hotson A, Keegan M, Schmelz EA, Mudgett MB (2008) XopD SUMO protease affects host transcription, promotes pathogen growth, and delays symptom development in xanthomonas-infected tomato leaves. *Plant Cell* 20: 1915-1929

Kirkin V, Lamark T, Johansen T, Dikic I (2009) NBR1 cooperates with p62 in selective autophagy of ubiquitinated targets. *Autophagy* 5: 732-733

Kliza K, Taumer C, Pinzuti I, Franz-Wachtel M, Kunzelmann S, Stieglitz B, Macek B, Husnjak K (2017) Internally tagged ubiquitin: a tool to identify linear polyubiquitin-modified proteins by mass spectrometry. *Nat Methods* 14: 504-512

Kovach ME, Elzer PH, Hill DS, Robertson GT, Farris MA, Roop RM, 2nd, Peterson KM (1995) Four new derivatives of the broad-host-range cloning vector pBBR1MCS, carrying different antibiotic-resistance cassettes. *Gene* 166: 175-176

Kubori T, Galan JE (2003) Temporal regulation of salmonella virulence effector function by proteasome-dependent protein degradation. *Cell* 115: 333-342

Lal NK, Thanasuwat B, Huang PJ, Cavanaugh KA, Carter A, Michelmore RW, Dinesh-Kumar SP (2020) Phytopathogen Effectors Use Multiple Mechanisms to Manipulate Plant Autophagy. *Cell Host Microbe* 28: 558-571 e556

Langin G, Gouguet P, Üstün S (2020) Microbial Effector Proteins - A Journey through the Proteolytic Landscape. *Trends Microbiol* 28: 523-535

Leary AY, Savage Z, Tumtas Y, Bozkurt TO (2019) Contrasting and emerging roles of autophagy in plant immunity. *Curr Opin Plant Biol* 52: 46-53

1480 Lei L, Stevens DM, Coaker G (2020) Phosphorylation of the Pseudomonas Effector AvrPtoB
1481 by Arabidopsis SnRK2.8 Is Required for Bacterial Virulence. *Mol Plant* 13: 1513-1522
1482 Lenz HD, Haller E, Melzer E, Kober K, Wurster K, Stahl M, Bassham DC, Vierstra RD, Parker
1483 JE, Bautor J *et al* (2011) Autophagy differentially controls plant basal immunity to biotrophic
1484 and necrotrophic pathogens. *Plant J* 66: 818-830
1485 Levine B, Mizushima N, Virgin HW (2011) Autophagy in immunity and inflammation. *Nature*
1486 469: 323-335
1487 Lorenz C, Büttner D (2009) Functional characterization of the type III secretion ATPase HrcN
1488 from the plant pathogen *Xanthomonas campestris* pv. *vesicatoria*. *J Bacteriol* 191: 1414-1428
1489 Lou L, Zhang P, Piao R, Wang Y (2019) Salmonella Pathogenicity Island 1 (SPI-1) and Its
1490 Complex Regulatory Network. *Front Cell Infect Microbiol* 9: 270
1491 Marshall RS, Vierstra RD (2018) Autophagy: The Master of Bulk and Selective Recycling.
1492 *Annu Rev Plant Biol* 69: 173-208
1493 Mesquita FS, Thomas M, Sachse M, Santos AJ, Figueira R, Holden DW (2012) The Salmonella
1494 deubiquitinase SseL inhibits selective autophagy of cytosolic aggregates. *PLoS Pathog* 8:
1495 e1002743
1496 Minina EA, Moschou PN, Vetukuri RR, Sanchez-Vera V, Cardoso C, Liu Q, Elander PH,
1497 Dalman K, Beganovic M, Lindberg Yilmaz J *et al* (2018) Transcriptional stimulation of rate-
1498 limiting components of the autophagic pathway improves plant fitness. *J Exp Bot* 69: 1415-
1499 1432
1500 Mostowy S (2013) Autophagy and bacterial clearance: a not so clear picture. *Cell Microbiol*
1501 15: 395-402
1502 Nagel MK, Kalinowska K, Vogel K, Reynolds GD, Wu Z, Anzenberger F, Ichikawa M,
1503 Tsutsumi C, Sato MH, Kuster B *et al* (2017) Arabidopsis SH3P2 is an ubiquitin-binding protein
1504 that functions together with ESCRT-I and the deubiquitylating enzyme AMSH3. *Proc Natl*
1505 *Acad Sci U S A* 114: E7197-E7204
1506 Nakagawa T, Kurose T, Hino T, Tanaka K, Kawamukai M, Niwa Y, Toyooka K, Matsuoka K,
1507 Jinbo T, Kimura T (2007) Development of series of gateway binary vectors, pGWBs, for
1508 realizing efficient construction of fusion genes for plant transformation. *J Biosci Bioeng* 104:
1509 34-41
1510 Pandey P, Leary AY, Tumtas Y, Savage Z, Dagvadorj B, Duggan C, Yuen EL,
1511 Sanguankiattichai N, Tan E, Khandare V *et al* (2021) An oomycete effector subverts host
1512 vesicle trafficking to channel starvation-induced autophagy to the pathogen interface. *Elife* 10
1513 Pohl C, Dikic I (2019) Cellular quality control by the ubiquitin-proteasome system and
1514 autophagy. *Science* 366: 818-822
1515 Schultink A, Qi T, Lee A, Steinbrenner AD, Staskawicz B (2017) Roq1 mediates recognition
1516 of the *Xanthomonas* and *Pseudomonas* effector proteins XopQ and HopQ1. *Plant J* 92: 787-
1517 795
1518 Schwanhausser B, Busse D, Li N, Dittmar G, Schuchhardt J, Wolf J, Chen W, Selbach M (2011)
1519 Global quantification of mammalian gene expression control. *Nature* 473: 337-342
1520 Singer AU, Schulze S, Skarina T, Xu X, Cui H, Eschen-Lippold L, Egler M, Srikumar T,
1521 Raught B, Lee J *et al* (2013) A pathogen type III effector with a novel E3 ubiquitin ligase
1522 architecture. *PLoS Pathog* 9: e1003121
1523 Svenning S, Lamark T, Krause K, Johansen T (2011) Plant NBR1 is a selective autophagy
1524 substrate and a functional hybrid of the mammalian autophagic adapters NBR1 and
1525 p62/SQSTM1. *Autophagy* 7: 993-1010
1526 Timilsina S, Potnis N, Newberry EA, Liyanapathiranage P, Iruegas-Bocardo F, White FF, Goss
1527 EM, Jones JB (2020) Xanthomonas diversity, virulence and plant-pathogen interactions. *Nat*
1528 *Rev Microbiol* 18: 415-427

Üstün S, Bartetzko V, Börnke F (2013) The *Xanthomonas campestris* type III effector XopJ targets the host cell proteasome to suppress salicylic-acid mediated plant defence. *PLoS Pathog* 9: e1003427

Üstün S, Bartetzko V, Börnke F (2015) The *Xanthomonas* effector XopJ triggers a conditional hypersensitive response upon treatment of N. benthamiana leaves with salicylic acid. *Front Plant Sci* 6: 599

Üstün S, Börnke F (2014) Interactions of *Xanthomonas* type-III effector proteins with the plant ubiquitin and ubiquitin-like pathways. *Front Plant Sci* 5: 736

Üstün S, Börnke F (2015) The *Xanthomonas campestris* type III effector XopJ proteolytically degrades proteasome subunit RPT6. *Plant Physiol* 168: 107-119

Üstün S, Hafrén A, Hofius D (2017) Autophagy as a mediator of life and death in plants. *Curr Opin Plant Biol* 40: 122-130

Üstün S, Hafrén A, Liu Q, Marshall RS, Minina EA, Bozhkov PV, Vierstra RD, Hofius D (2018) Bacteria Exploit Autophagy for Proteasome Degradation and Enhanced Virulence in Plants. *Plant Cell* 30: 668-685

Üstün S, Hofius D (2018) Anti- and pro-microbial roles of autophagy in plant-bacteria interactions. *Autophagy* 14: 1465-1466

Üstün S, Konig P, Guttman DS, Börnke F (2014) HopZ4 from *Pseudomonas syringae*, a member of the HopZ type III effector family from the YopJ superfamily, inhibits the proteasome in plants. *Mol Plant Microbe Interact* 27: 611-623

Üstün S, Sheikh A, Gimenez-Ibanez S, Jones A, Ntoukakis V, Börnke F (2016) The Proteasome Acts as a Hub for Plant Immunity and Is Targeted by *Pseudomonas* Type III Effectors. *Plant Physiol* 172: 1941-1958

van Wijk SJ, Fiskin E, Putyrski M, Pampaloni F, Hou J, Wild P, Kensche T, Grecco HE, Bastiaens P, Dikic I (2012) Fluorescence-based sensors to monitor localization and functions of linear and K63-linked ubiquitin chains in cells. *Mol Cell* 47: 797-809

Yan Y, Wang P, He C, Shi H (2017) MeWRKY20 and its interacting and activating autophagy-related protein 8 (MeATG8) regulate plant disease resistance in cassava. *Biochem Biophys Res Commun* 494: 20-26

Yang Y, Klionsky DJ (2020) Autophagy and disease: unanswered questions. *Cell Death Differ* 27: 858-871

Zeng H, Xie Y, Liu G, Lin D, He C, Shi H (2018) Molecular identification of GAPDHs in cassava highlights the antagonism of MeGAPCs and MeATG8s in plant disease resistance against cassava bacterial blight. *Plant Mol Biol* 97: 201-214

Zhang Y, Higashide W, Dai S, Sherman DM, Zhou D (2005) Recognition and ubiquitination of Salmonella type III effector SopA by a ubiquitin E3 ligase, HsRMA1. *J Biol Chem* 280: 38682-38688

Zheng YT, Shahnazari S, Brech A, Lamark T, Johansen T, Brumell JH (2009) The adaptor protein p62/SQSTM1 targets invading bacteria to the autophagy pathway. *J Immunol* 183: 5909-5916

Zhou J, Wang J, Cheng Y, Chi YJ, Fan B, Yu JQ, Chen Z (2013) NBR1-mediated selective autophagy targets insoluble ubiquitinated protein aggregates in plant stress responses. *PLoS Genet* 9: e1003196

Zhuang X, Jiang L (2014) Autophagosome biogenesis in plants: roles of SH3P2. *Autophagy* 10: 704-705

Zhuang X, Wang H, Lam SK, Gao C, Wang X, Cai Y, Jiang L (2013) A BAR-domain protein SH3P2, which binds to phosphatidylinositol 3-phosphate and ATG8, regulates autophagosome formation in Arabidopsis. *Plant Cell* 25: 4596-4615

1579 ## Supporting information

1580

1581 **Figure S1: S**ilencing of *ATG7* in *N. benthamiana* plants abolishes autophagosome formation
1582 and Xcv blocks autophagy at 6hpi.
1583 **Figure S2:** Virus induced gene silencing of *ATG7* in *N. benthamiana* is beneficial for Xcv.
1584 **Figure S3:** Suppression of autophagy is enhanced by T3Es**.**
1585 **Figure S4:** Screening for Xanthomonas T3Es with altered autophagic flux.
1586 **Figure S5:** XopL contributes to Xcv virulence.
1587 **Figure S6:** Joka2 bodies are induced during Xcv infection in a XopL-dependent manner.
1588 **Figure S7:** Transgenic *A. thaliana* GFP-XopL plants display defects in autophagic degradation.
1589 **Figure S8**: SH3P2 is conserved in different plant species.
1590 **Figure S8:** XopL is ubiquitinated *in planta*.
1591 **Supplemental Video 1:** XopL/SH3P2 puncta are mobile.
1592 **Figure S9:** Silencing of SH3P2 in *N. benthamiana* perturbs autophagy.
1593 **Figure S10:** Gene expression of SH3P2 is induced by XopL and XopL-mediated degradation
1594 is due to post-transcriptional degradation events.
1595 **Figure S11:** RFP-XopL ΔE3 co-localizes with and is unable to ubiquitinate SH3P2-GFP.
1596 **Figure S12:** XopL is degraded in the vacuole.
1597 **Figure S13:** Virus-induced gene silencing of *Joka2* in *N. benthamiana* plants.
1598 **Figure S14:** XopL in planta ubiquitination is enhanced by the presence of AIMp.
1599 **Figure S15:** XopL is ubiquitinated *in planta* and undergoes self-ubiquitination.
1600 **Figure S16**: Characterization of $XopL_{K191A}$ variant i*n vitro* and *in planta*.
1601 **Figure S17:** XopL ΔE3 is degraded by autophagy.
1602 **Figure S18:** XopL K191 residue is highly conserved through the Xanthomonas genus
1603 **Supplemental Table 1**: Primers used in manuscript.
1604
1605
1606
1607
1608
1609
1610
1611
1612
1613
1614
1615
1616
1617
1618
1619
1620
1621
1622
1623
1624
1625
1626
1627
1628

1629 **Supplemental Figure 1**

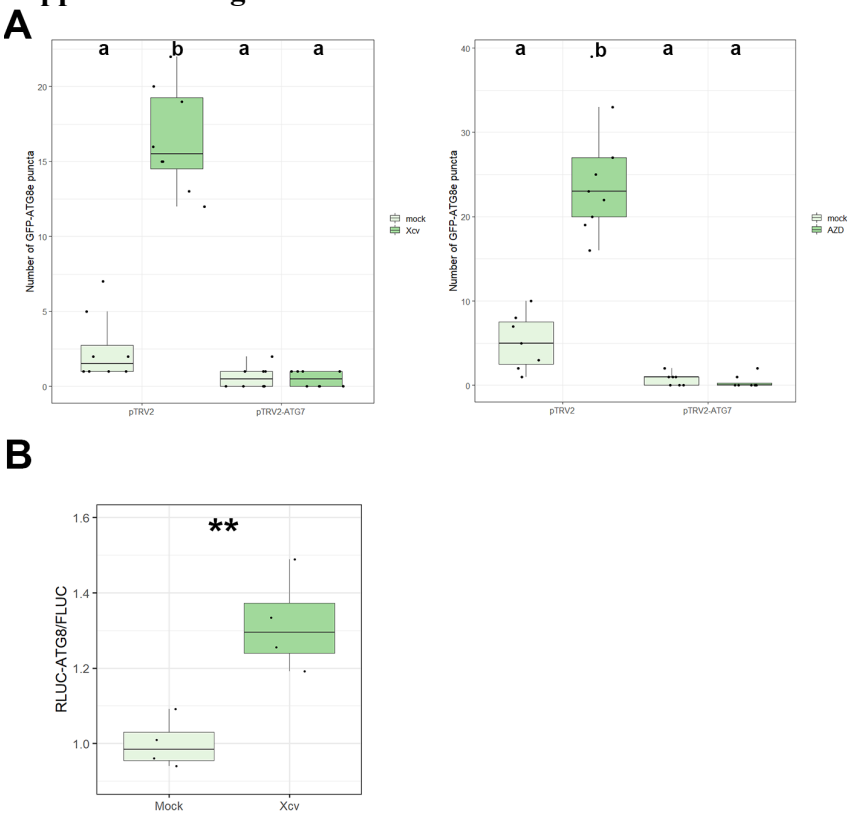


1630
1631 **Fig. S1: Silencing of *ATG7* in *N. benthamiana* plants abolishes autophagosome formation**
1632 **and Xcv blocks autophagy at 6hpi.** GFP-ATG8e-labeled puncta were quantified from plants
1633 silenced for *ATG7* (pTRV2-ATG7) infected with mock or Xcv *ΔxopQ* at 6hpi in the presence
1634 or absence of ConA, and of AZD. Puncta were calculated from z-stacks (X) of *n*=12 individuals
1635 using ImageJ. Different letters indicate statistically significant different groups ($P < 0.05$) as
1636 determined by one way ANOVA.
1637 **(B)** RLUC-ATG8a or RLUC-NBR1 constructs were coexpressed with internal control FLUC
1638 in *N. benthamiana*. *Xcv ΔxopQ* or infiltration buffer (mock) was co-infiltrated with
1639 Agrobacteria containing the respective constructs. RLUC and FLUC activities were
1640 simultaneously measured in leaf extracts at 8 h post- infiltration using the dual-luciferase
1641 system. Values represent the ratio of RLUC-ATG8a and FLUC activities (n=4). Statistical
1642 significance (***$P < 0.001$) was revealed by Student's *t*-test. The experiment was repeated 3
1643 times with similar results.
1644
1645 **Supplemental Figure 2**
1646

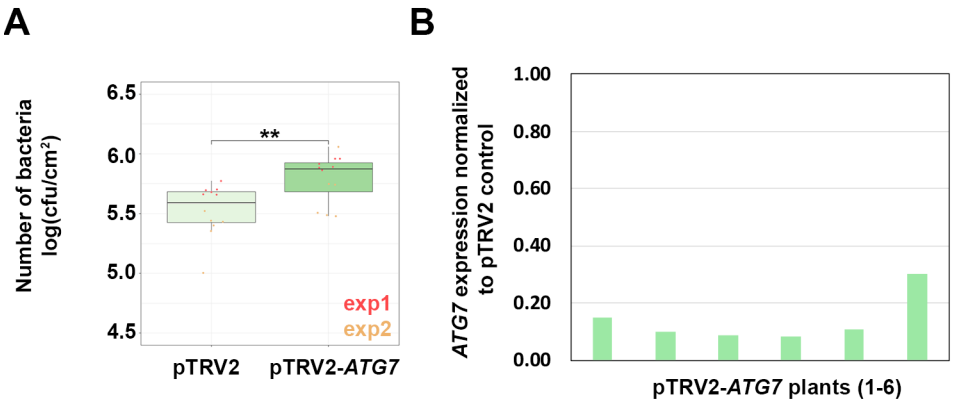


1647

**Fig. S2: Virus induced gene silencing of *ATG7* in *N. benthamiana* is beneficial for Xcv.**
**(A)** Growth of Xcv *ΔxopQ* in *N. benthamiana* plants silenced for *ATG7* (pTRV2-*ATG7*) compared to control plants (pTRV2). Leaves were dip-inoculated with a bacteria suspension at $OD_{600}$ = 0.2 and bacteria were quantified at 6 dpi. Data represent the mean SD (n = 6). Significant differences were calculated using Student's *t-test* and are indicated by **, P < 0.01. The experiment was repeated twice with similar trends. Red and yellow data points represent repeats of the experiment.
**(B)** qRT-PCR analysis of *ATG7* mRNA levels in silenced *N. benthamiana* plants. *Actin* expression was used to normalize the expression value in each sample, and relative expression values were determined against the mean expression in pTRV2 (control) plants**.**

**Supplemental Figure 3**

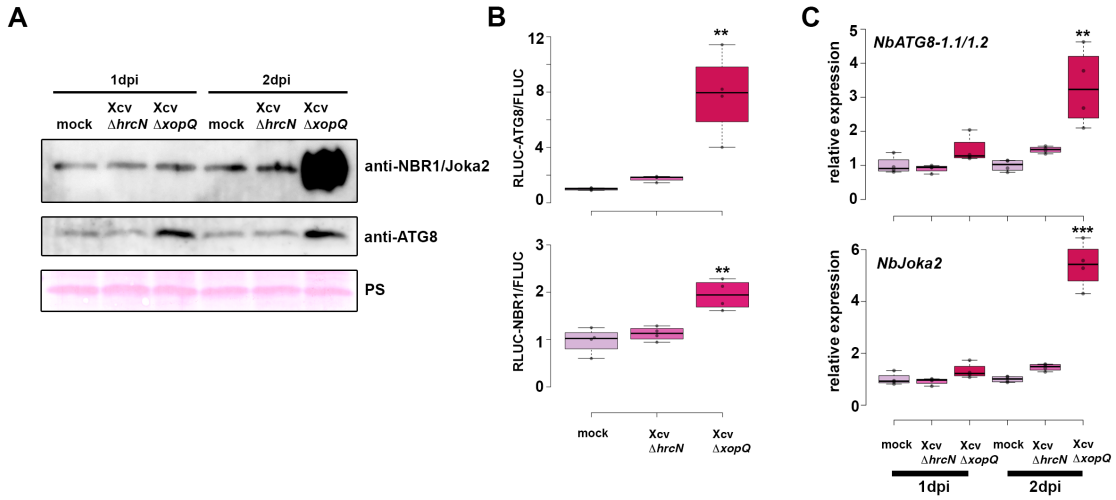


**Fig. S3: Suppression of autophagy is enhanced by T3Es.**
**(A)** Immunoblot analysis of NBR1 and ATG8 protein levels in Xcv *ΔxopQ, ΔhrcN* or mock infected *N. benthamiana* plants at 1 and 2dpi. Ponceau Staining (PS) served as a loading control. The experiment was repeated twice with similar results.
**(B)** Autophagic flux determined by quantitative dual-luciferase assay. RLUC-ATG8a or RLUC-NBR1 constructs were coexpressed with internal control FLUC in *N. benthamiana*. Xcv *ΔxopQ* and *ΔhrcN* were respectively co-infiltrated with Agrobacteria containing the luciferase constructs. *Renilla* and *Firefly* luciferase activities were simultaneously measured in leaf extracts at 48 h post- infiltration using the dual-luciferase system. Values represent the ratio of RLUC-ATG8a and FLUC activities normalized to mock (n=4). Statistical significance (**$P$<0.01) was revealed by Student's *t*-test. The experiment was repeated 2 times with similar results.
**(C)** RT-qPCR analysis of *NbATG8-1.1/2* and *NbJoka2* transcript levels upon challenge of *N. benthamiana* plants with Xcv *ΔxopQ* and *ΔhrcN* for 1 and 2 dpi compared to mock infected plants. Values represent expression relative to mock control of respective time point and were normalized to *actin*. Statistical significance (*** $P$ < 0.001) was revealed by Student's *t*-test.

1686 **Supplemental Figure 4**
1687

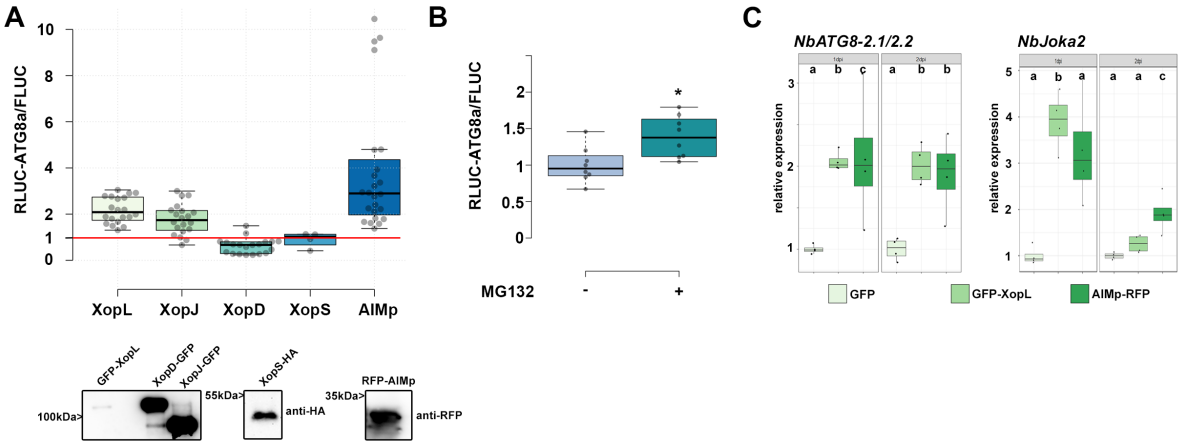


1688
1689
1690 **Fig. S4: Screening for Xanthomonas T3Es with altered autophagic flux.**
1691 **(A)** RLUC-ATG8a constructs were coexpressed with internal control FLUC in *N. benthamiana*.
1692 GFP-XopL, XopJ-GFP, XopD-GFP and XopS-HA were co-infiltrated with Agrobacteria
1693 carrying the RLUC-ATG8a and FLUC constructs. Renilla and Firefly luciferase activities were
1694 simultaneously measured in leaf extracts at 48 h post- infiltration using the dual-luciferase
1695 system. Values represent the ratio of RLUC-ATG8a to FLUC activity normalized to GFP
1696 control (XopL, XopJ, XopD, AIMp; n=20; XopS n=4). Expression of T3Es and RFP-AIMp
1697 were verified with the indicated antibodies.
1698 **(B)** RLUC-ATG8a constructs were coexpressed with internal control FLUC in *N. benthamiana*.
1699 Plants were treated with MG132 for 6 hours prior measurement. Values represent the ratio of
1700 RLUC-ATG8a to FLUC activity normalized to vector control (n=8). Statistical significance (*
1701 $P < 0.5$) was revealed by Student's *t*-test.
1702 **(C)** RT-qPCR analysis of *NbATG8-2.1/2* and *NbJoka2* transcript levels upon Agrobacteria-
1703 mediated transient expression of GFP, GFP-XopL or AIMp for 1 and 2 dpi. Values represent
1704 expression relative to GFP control of respective time point and were normalized to *actin*.
1705 Statistical significantly different groups are denoted by different letters, as calculated using
1706 Kruskal-Wallis rank sum test ($P<0.05$).
1707
1708 **Supplemental Figure 5**

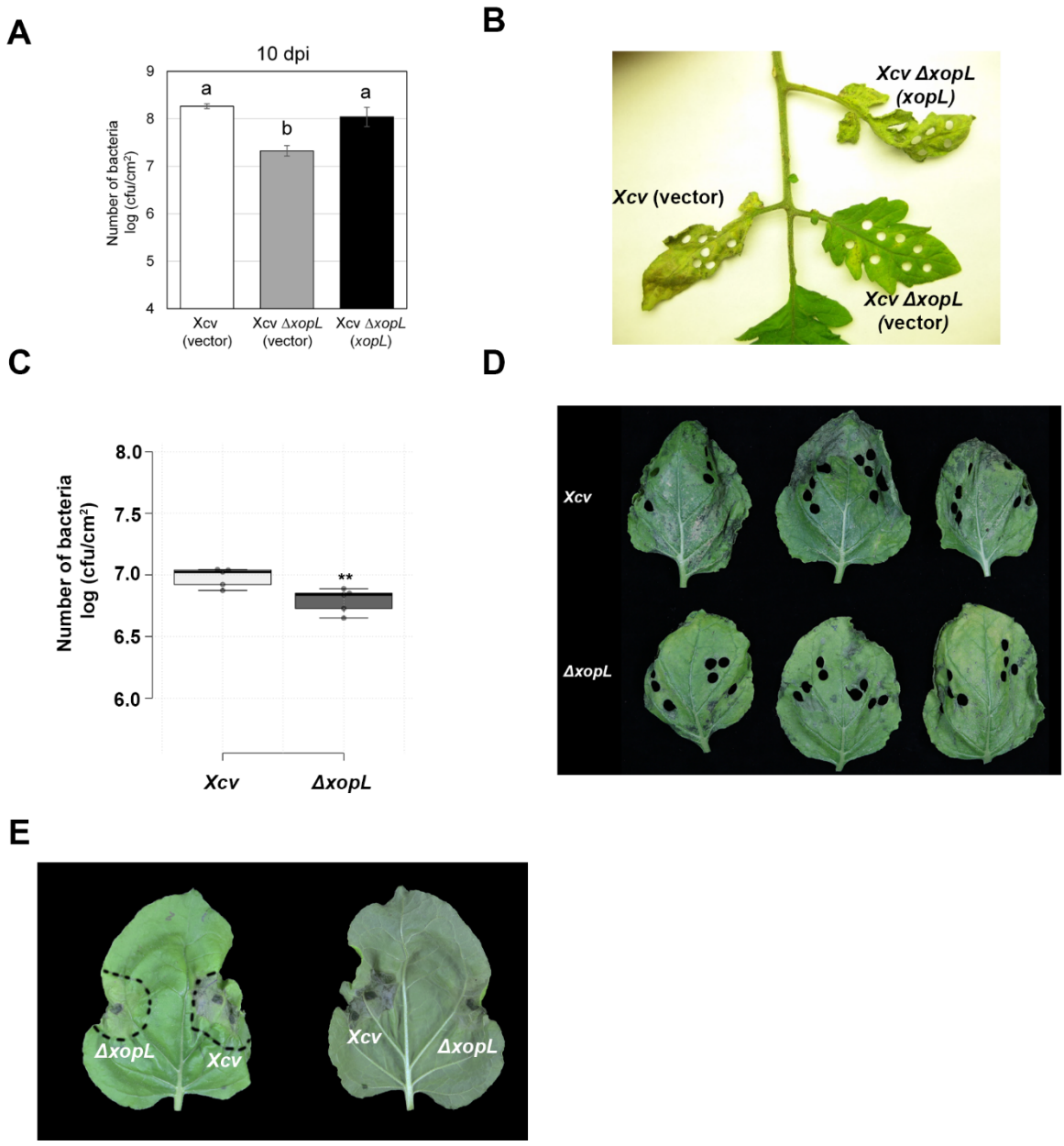


**Fig. S5: XopL contributes to Xcv virulence.**
**(A)** Growth of Xcv 85-10 (vector) (white bar), Xcv 85-10 Δ*xopL* (vector) (grey bar), and Xcv 85-10 Δ*xopL* (*xopL*) (black bar) strains in tomato VF36 leaves. Leaves were dipped in a 2 x $10^8$ CFU/mL suspension of bacteria. The number of bacteria in each leaf was quantified at 10 dpi. Data points represent mean $\log_{10}$ colony-forming units per $cm^2$ ± SD of three plants. Different letters above bars indicate statistically significant (Tukey's honestly significant difference (HSD) test, $P < 0.05$) differences between samples. Vector = pBBR1MCS-2.
**(B)** Delayed disease symptom development in tomato leaves inoculated with *Xcv* or *Xcv* Δ*xopL*. Tomato leaves inoculated with strains described in (A) were photographed at 14 dpi.
**(C)** Growth of Xcv 85-10, Xcv 85-10 Δ*xopL* strains in *roq1 N. benthamiana* leaves. Leaves were dipped in a 2 x $10^8$ CFU/mL suspension of bacteria. The number of bacteria in each leaf was quantified at 10 dpi (n = 5). Significant differences were calculated using Student's *t-test* (**, $P < 0.01$). The experiment was repeated twice with similar trends.

**(D)** Delayed disease symptom development in *roq1 N. benthamiana* leaves dip-inoculated with *Xcv* or *Xcv* Δ*xopL*. *N. benthamiana roq1* leaves inoculated with strains described in (C) were photographed at 10 dpi.
**(E)** Delayed symptom development in *roq1 N. benthamiana* leaves inoculated with *Xcv* or *Xcv* Δ*xopL*. Leaves were syringe-inoculated with $OD_{600}$=0.2 and photographed at 3 dpi.

**Supplemental Figure 6**

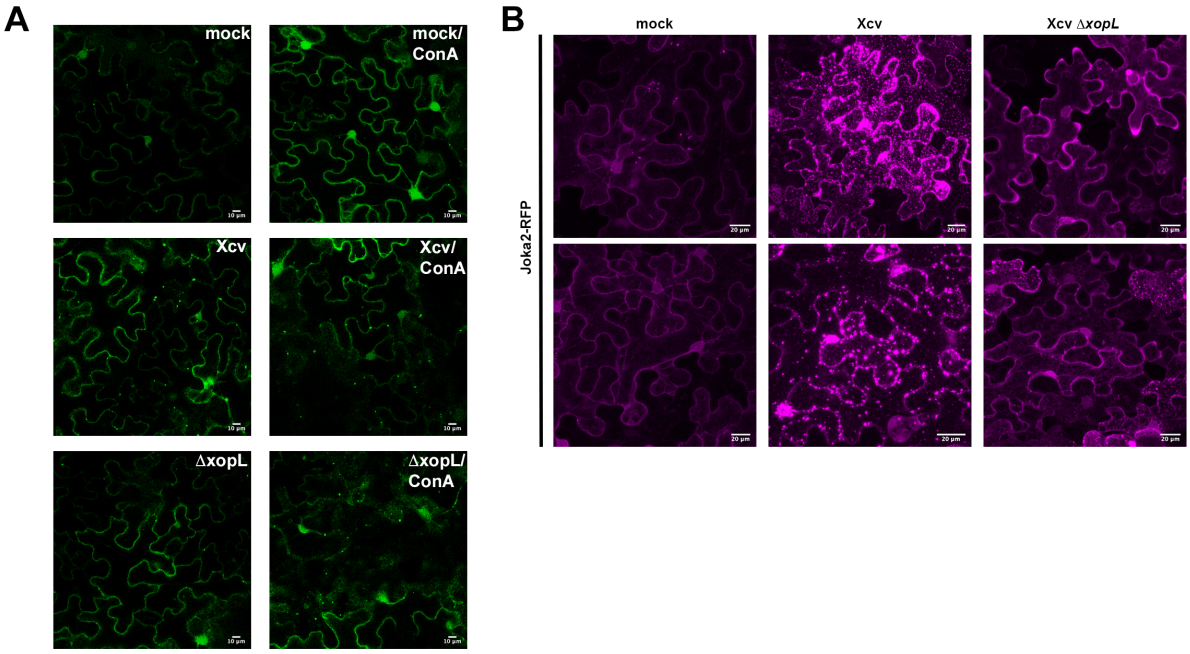


**Fig. S6: Joka2 bodies are induced during Xcv infection in a XopL-dependent manner.**
**(A)** GFP-ATG8e-labeled autophagosomes imaged from *N. benthamiana* plants infected with mock, Xcv or *Xcv* Δ*xopL* at 2 dpi in the presence or absence of ConA (bars = 10 µm).
**(B)** RFP-Joka2 labelled puncta or aggregates upon challenge of *N. benthamiana* leaves with mock, *Xcv* or *Xcv* Δ*xopL* infection at 1dpi.

**Supplemental Figure 7**

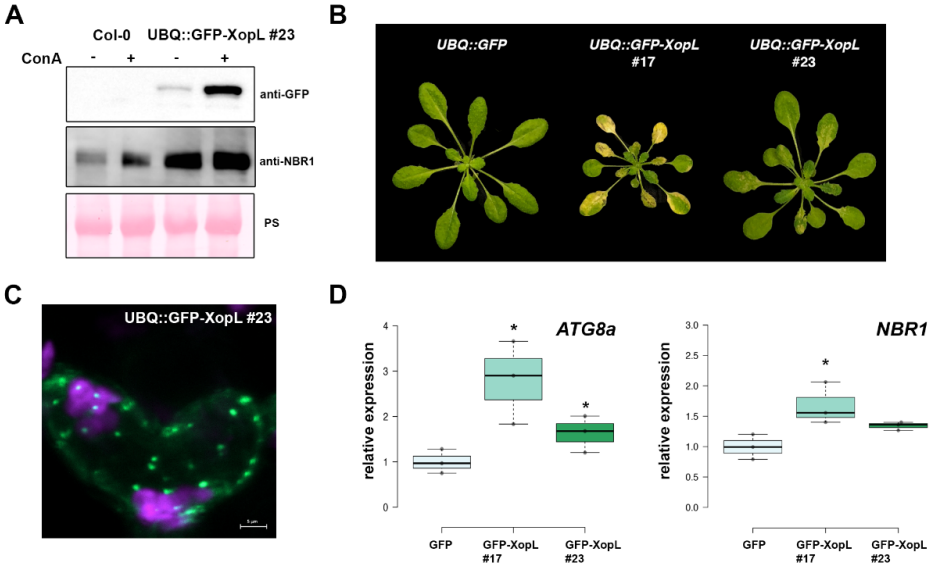

**Fig. S7: Transgenic *A. thaliana* GFP-XopL plants display defects in autophagic degradation**

**(A)** Immunoblot analysis of NBR1 protein levels in transgenic UBQ::GFP-XopL plants or Col-0. Plants were treated with concanamycin A (ConA) for 6 hours. Expression of GFP-XopL was verified with an anti-GFP antibody. Ponceau S staining serves as a loading control.

**(B)** 5 weeks old *A. thaliana* plants expressing UBQ::GFP-XopL develop an early senescence phenotype reminiscent of autophagy deficient mutants.

**(C)** Localization analysis of GFP-XopL of transgenic *A. thaliana* UBQ::GFP-XopL #23 line. Image represents single confocal planes from abaxial epidermal cells (bars = 5 µm).

**(D)** RT-qPCR analysis of *ATG8a* and *NBR1* transcript levels in *Arabidopsis thaliana* GFP or GFP-XopL plants. Values represent expression (n=3) relative to GFP control and were normalized to *PP2A*. Statistical significance (**P*<0.05) was revealed by Student's *t*-test.

**Supplemental Figure 8**

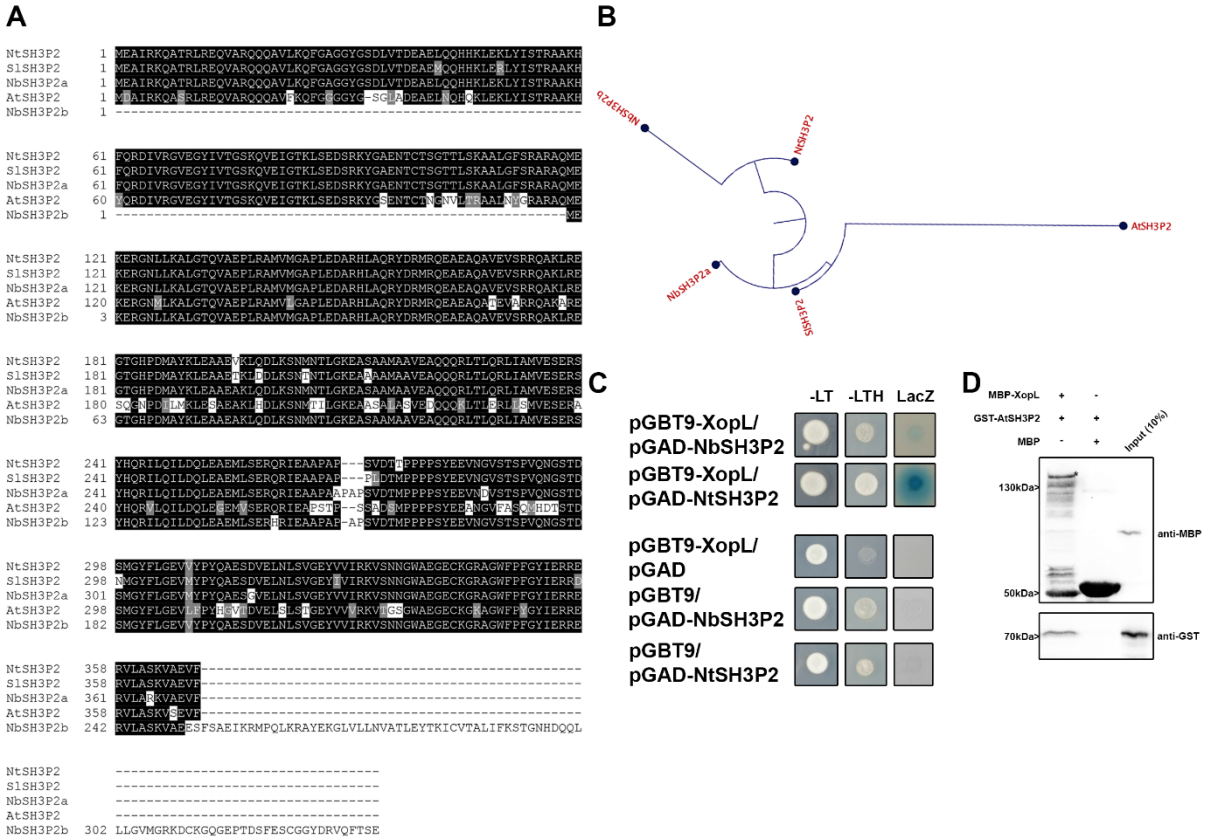


**Fig. S8: SH3P2 is conserved in different plant species.**

**(A)** Protein sequence alignment of SH3P2 from different species. The alignment was generated using CLUSTALW2 with default parameters and BoxShade 3.21. Positions of identical and similar sequences are boxed in black and grey, respectively. The following sequences were used to build the alignment: *Arabidopsis thaliana*, *Nicotiana tabacum, Nicotiana benthamiana*, *Solanum lycopersicum*.

**(B)** Phylogentic analysis of the SH3P2 from different plant species.

**(C)** XopL interacts with SH3P2 from *Nicotiana tabacum* and *Nicotiana benthamiana*. Interaction of XopL with SH3P2 in yeast two-hybrid assays. XopL fused to the GAL4 DNA-binding domain was expressed in combination with SH3P2 fused to the GAL4 activation domain (AD) in yeast strain Y190. Cells were grown on selective media before a LacZ filter

assay was performed. The empty AD or BD vector served as negative control. NtSH3P2 = *Nicotiana tabacum* SH3P2, NbSH3P2 = *Nicotiana benthamiana* –LT = yeast growth on medium without Leu and Trp, –HLT = yeast growth on medium lacking His, Leu, and Trp, indicating expression of the HIS3 reporter gene. LacZ, activity of the lacZ reporter gene.
**(D)** *In vitro* co-IP assay showing direct interaction of XopL with AtSH3P2. MBP-XopL and GST-AtSH3P2 were expressed in E. coli. Pull down was performed using amylose resin. Proteins were detected in an immunoblot using antibodies as indicated.

**Supp Video 1: XopL/SH3P2 puncta are mobile**
*Nicotiana benthamiana* leaf epidermal cells transiently expressing Venus$^{N173}$-XopL in combination with AtSH3P2-Venus$^{C155}$.

**Supplemental Figure 9**

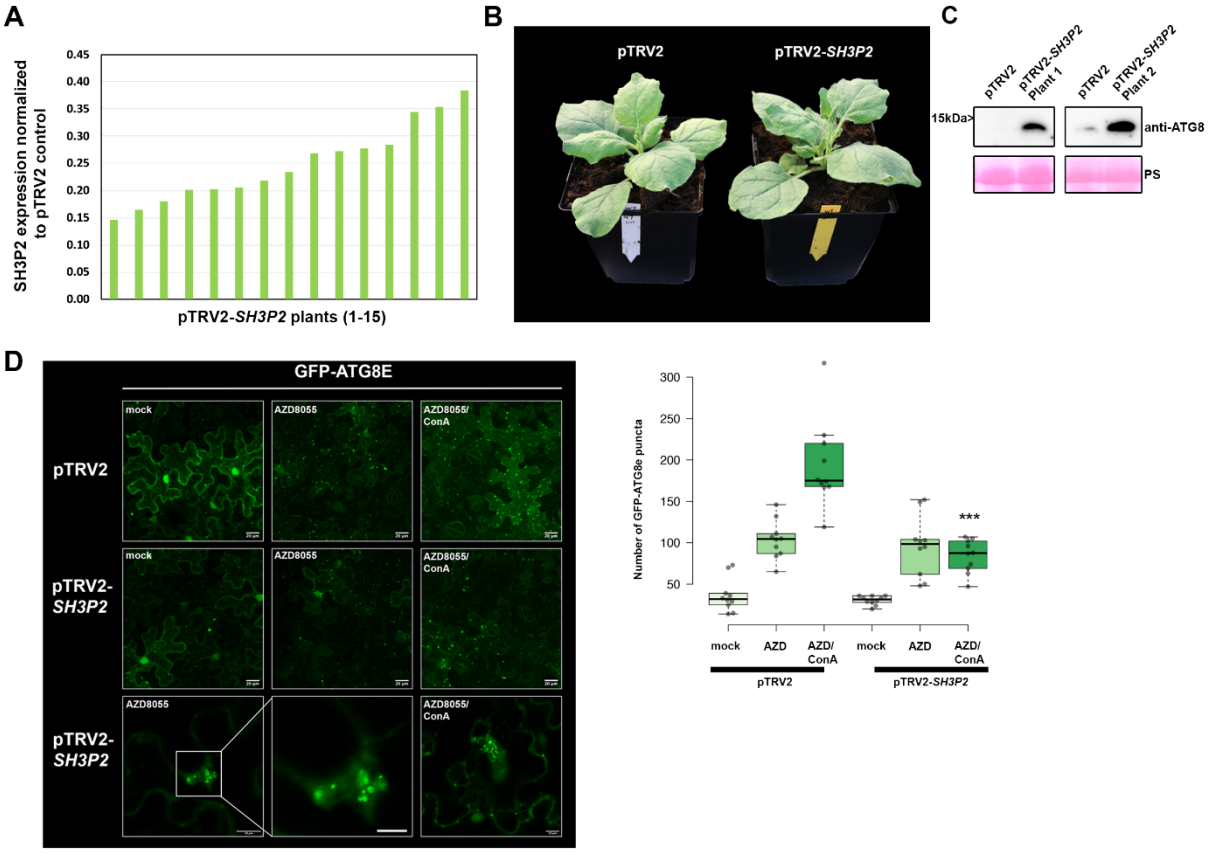


**Fig. S9: Silencing of SH3P2 in *N. benthamiana* perturbs autophagy.**
**(A)** qRT-PCR analysis of SH3P2 mRNA levels in silenced plants. *Actin* expression was used to normalize the expression value in each sample, and relative expression values were determined against pTRV2 control plants (set to 1).
**(B)** Phenotype of SH3P2-VIGS plants in comparison to the pTRV2 control. Picture was taken 14 dpi.
**(C)** Immunoblot analysis of ATG8 protein levels in *N. benthamiana* pTRV2 (control) and pTRV2-*SH3P2* (*SH3P2* silencing) 2 weeks after VIGS. Ponceau Staining (PS) served as a loading control. The experiment was repeated twice with similar results.
**(D)** GFP-ATG8e-labeled autophagosomes were quantified from pTRV2 or pTRV2-SH3P2 plants transiently expressing GFP-ATG8e at 2dpi in the presence of autophagy inducer AZD = AZD8055 and AZD/ConA. Puncta were calculated from z-stacks of *n*=10 individuals using

ImageJ. Statistical significance (*** $P < 0.5$) was revealed by Student's *t*-test comparing number of autophagosomes in AZD/ConA treatments in pTRV2 and pTRV2-*SH3P2* plants. The experiment was repeated twice with similar results.

**Supplemental Figure 10**

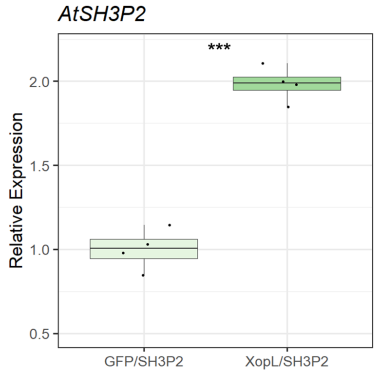


**Fig. S10: Gene expression of SH3P2 is induced by XopL and XopL-mediated degradation is due to post-transcriptional degradation events.**
**(A)** qRT-PCR analysis of AtSH3P2-specific mRNA levels in *N. benthamiana* plants transiently expressing AtSH3P2-HA, upon coexpression with GFP or GFP-XopL. *Actin* expression was used to normalize the expression value in each sample. Values represent *AtSH3P2* transcript level normalized to control (n=4).

**Supplemental Figure 11**

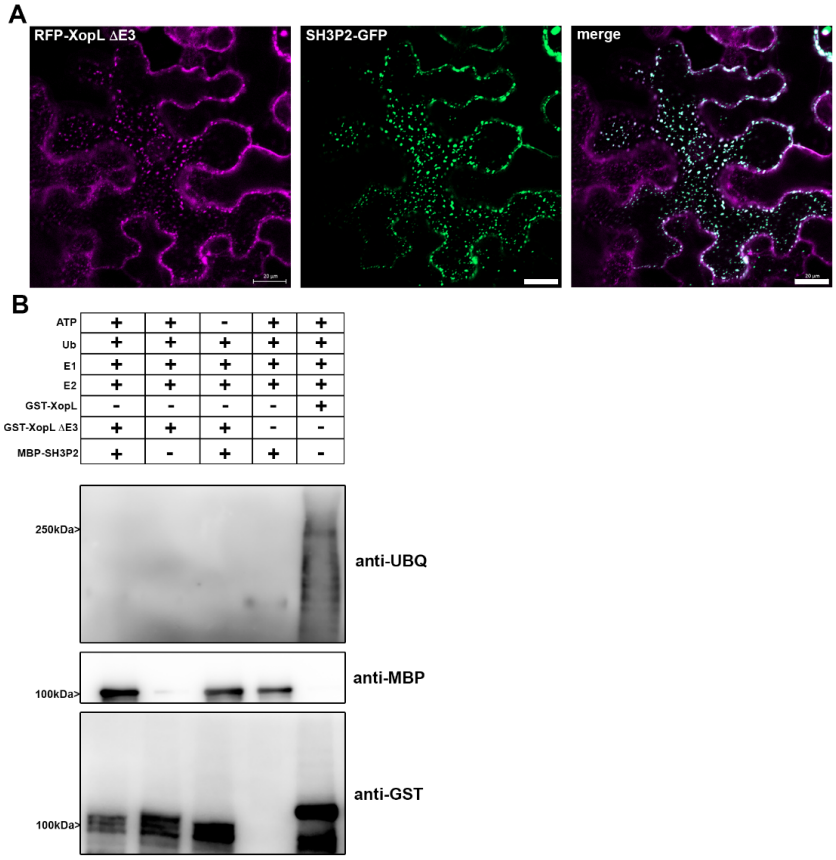


**Fig. S11: RFP-XopL ΔE3 co-localizes with and is unable to ubiquitinate SH3P2-GFP.**

1817 **(A)** Colocalization analysis of RFP-XopL ΔE3 with SH3P2-GFP in *N. benthamiana* leaves.
1818 Imaging was performed 2 d after transient expression and images represent single confocal
1819 planes from abaxial epidermal cells (bars = 20 µm).
1820 **(B)** *In vitro* ubiquitination assay reveals GST-XopL ΔE3 is unable to ubiquitinate MBP-SH3P2.
1821 GST-XopL, ΔE3 and MBP-SH3P2 were tested using the Arabidopsis His-AtUBA1 and His-
1822 AtUBC8. Lanes 2 to 4 are negative controls, while Lane 5 is the positive control with GST-
1823 XopL. Proteins were separated by SDS-PAGE and detected by immunoblotting using the
1824 indicated antibodies. The experiment was repeated three times with similar results.
1825
1826 **Supplemental Figure 12**

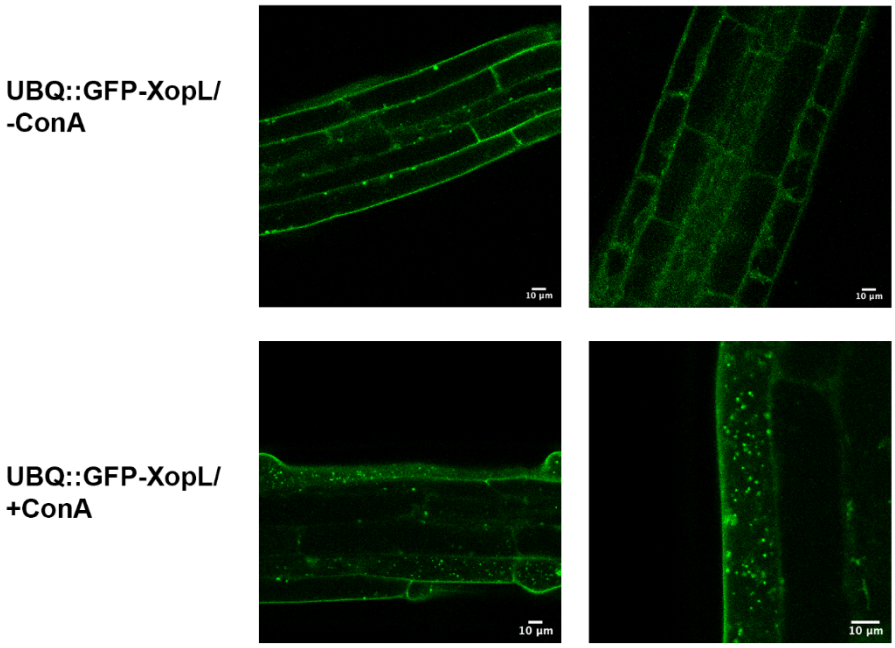


1827
1828 **Fig. S12: XopL is degraded in the vacuole**. Localization of GFP-XopL in the presence or
1829 absence of ConA in transgenic GFP-XopL. DMSO or 0.5 µM ConA was used to treat seedlings,
1830 followed by confocal imaging of the roots. GFP-labeled puncta detectable upon ConA treatment
1831 indicate XopL accumulation in the vacuole (bars = 20 µm).
1832
1833 **Supplemental Figure 13**
1834

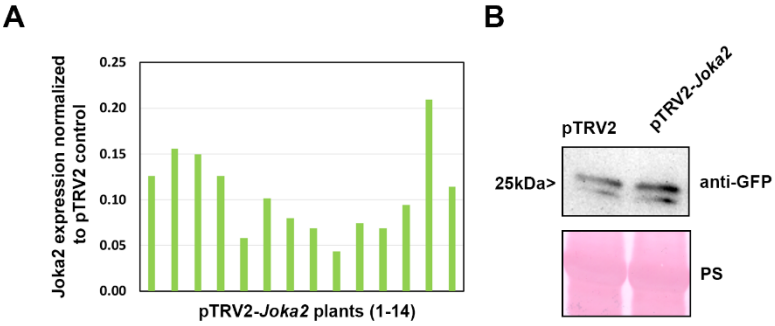


1835
1836
1837 **Fig. S13: Virus-induced gene silencing of *Joka2* in *N. benthamiana* plants.**

1838 **(A)** qRT-PCR analysis of Joka2 mRNA levels in *Joka2* silenced pepper plants. *Actin* expression
1839 was used to normalize the expression value in each sample, and relative expression values were
1840 determined against pTRV2 control plants (set to 1)**.**
1841 **(B)** Immunoblot analysis of GFP and GFP-XopL protein levels in *N. benthamiana* plants
1842 silenced for *Joka2* (pTRV2-Joka2) compared against control (pTRV2). Ponceau staining (PS)
1843 served as a loading control.
1844
1845 **Supplemental Figure 14**
1846

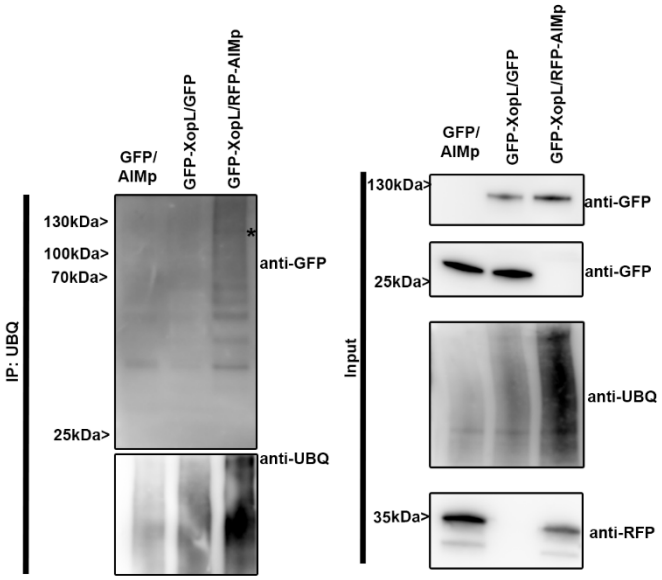


1847
1848 **Fig. S14: XopL in planta ubiquitination is enhanced by the presence of AIMp** GFP-XopL
1849 or GFP were transiently expressed in *N. benthamiana*. RFP-AIMp was co-infiltrated. Samples
1850 were taken 48 hpi, and total proteins (Input) were subjected to immunoprecipitation (IP) with
1851 the ubiquitin pan selector, followed by immunoblot analysis of the precipitates using either anti-
1852 GFP or anti-ubiquitin antibodies. RFP-AIMp expression was verified by an anti-RFP antibody.
1853 Asterisk indicates the GFP-XopL full-length protein. The experiment was repeated twice with
1854 similar results.
1855
1856 **Supplemental Figure 15**
1857

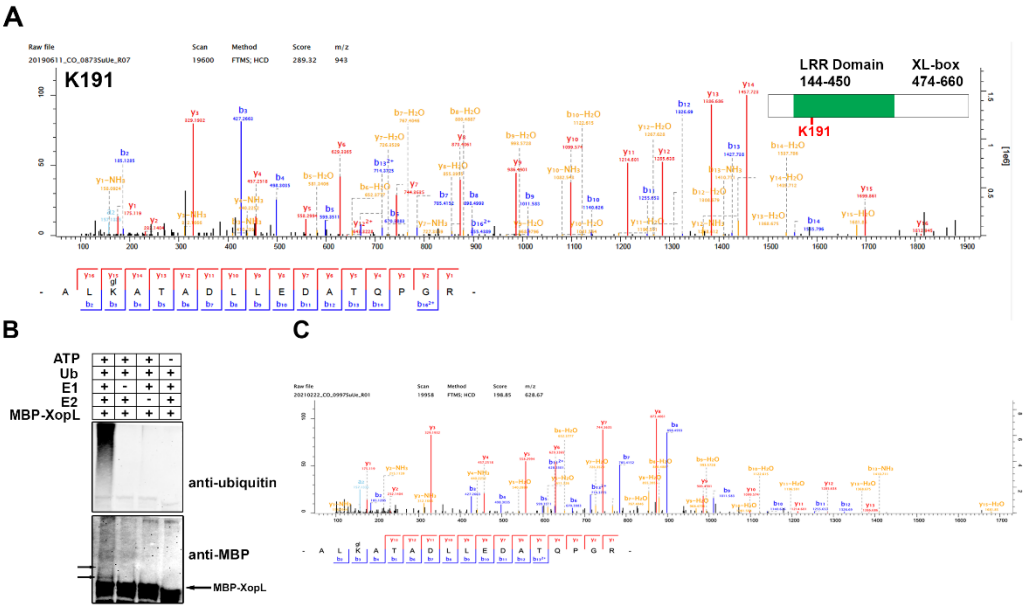


**Fig. S15: XopL is ubiquitinated *in planta* and undergoes self-ubiquitination**

**(A)** XopL ubiquitination site at lysine 191 was identified in vivo by LC-MS/MS. GFP-XopL was transiently expressed in *N. benthamiana* and total proteins were subjected to anti-GFP IP followed by trypsin digestion. Ubiquitinated peptides were detected by LC-MS/MS. The spectrum shows the fragmentation pattern of the GlyGly modified peptide ALglKATADLLEDATQPGR corresponding to amino acids 189-205.

**(B)** *In vitro* ubiquitination assay reveals autoubiquitination of XopL. Ubiquitination of MBP-XopL was tested using the Arabidopsis His-AtUBA1 and His-AtUBC8. Lanes 2 to 4 are negative controls. Proteins were separated by SDS-PAGE and detected by immunoblotting using the indicated antibodies. Arrows in the MBP blot indicate higher molecular weight bands of MBP-XopL and autoubiquitination events. The experiment was repeated twice with similar results.

**(C)** XopL ubiquitination site at lysine 191 was identified in vitro by LC-MS/MS. GST-XopL was used in an in vitro ubiquitination assay and samples were subjected to trypsin digestion. Ubiquitinated peptides were detected by LC-MS/MS. The spectrum shows the fragmentation pattern of the GlyGly modified peptide ALglKATADLLEDATQPGR corresponding to amino acids 189-205.

**Supplemental Figure 16**

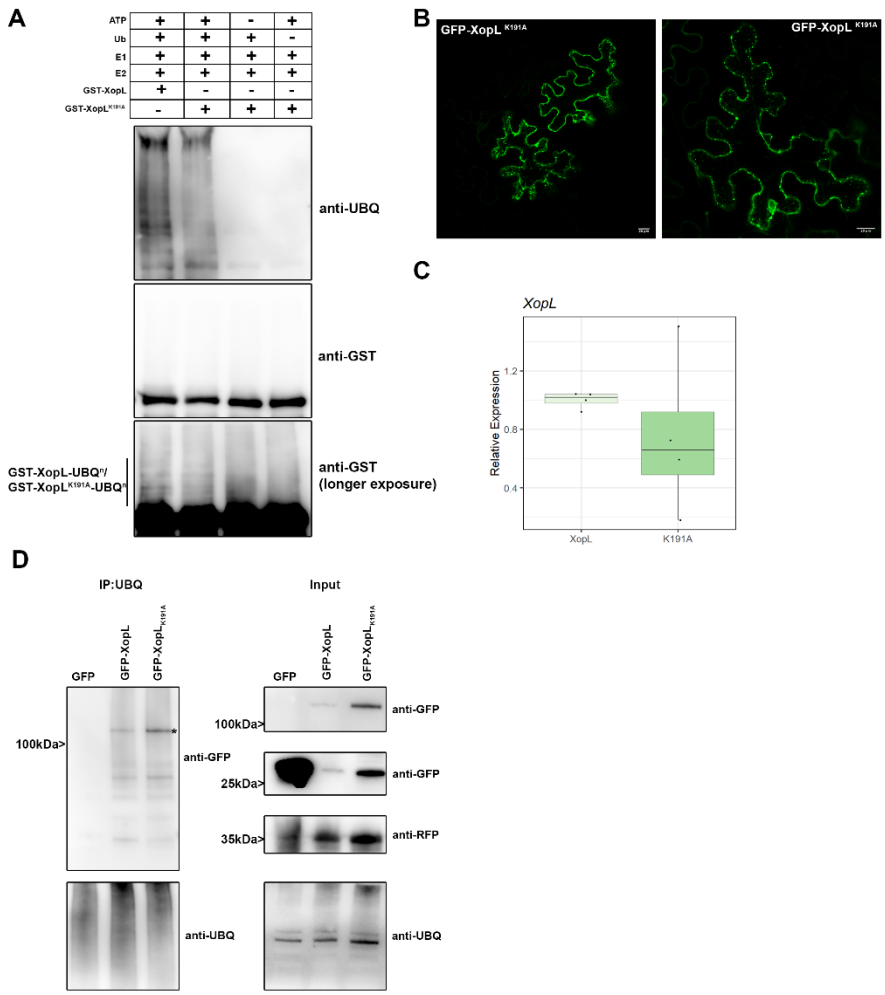


**Fig. S16: Characterization of XopL K191A variant in vitro and in planta.**
**(A)** *In vitro* ubiquitination assay reveals less autoubiquitination of XopL K191A compared to XopL WT. Ubiquitination of GST-XopL was tested using the Arabidopsis His-AtUBA1 and His-AtUBC8. Lanes 3 to 5 are negative controls. Proteins were separated by SDS-PAGE and detected by immunoblotting using the indicated antibodies. The experiment was repeated twice with similar results.
**(B)** Localization analysis of GFP-XopL$_{K191A}$ in *N. benthamiana* leaves. Imaging was performed 2 d after transient expression and images represent single confocal planes from abaxial epidermal cells (bars = 20 µm).
**(C)** qRT-PCR analysis of GFP-XopL and GFP-XopL K191A mRNA levels in *N. benthamiana* plants during transient expression. *Actin* expression was used to normalize the expression value in each sample.
**(D)** GFP-XopL and GFP-XopL$_{K191A}$ were transiently expressed in *N. benthamiana*. RFP-AIMp was co-infiltrated. Samples were taken 48 hpi, and total proteins (Input) were subjected to immunoprecipitation (IP) with the ubiquitin pan selector, followed by immunoblot analysis of the precipitates using either anti-GFP or anti-ubiquitin antibodies. GFP served as a control. RFP-AIMp expression was verified by an anti-RFP antibody. Asterisk indicates the GFP-XopL full-length protein. The experiment was repeated twice with similar results.

**Supplemental Figure 17**

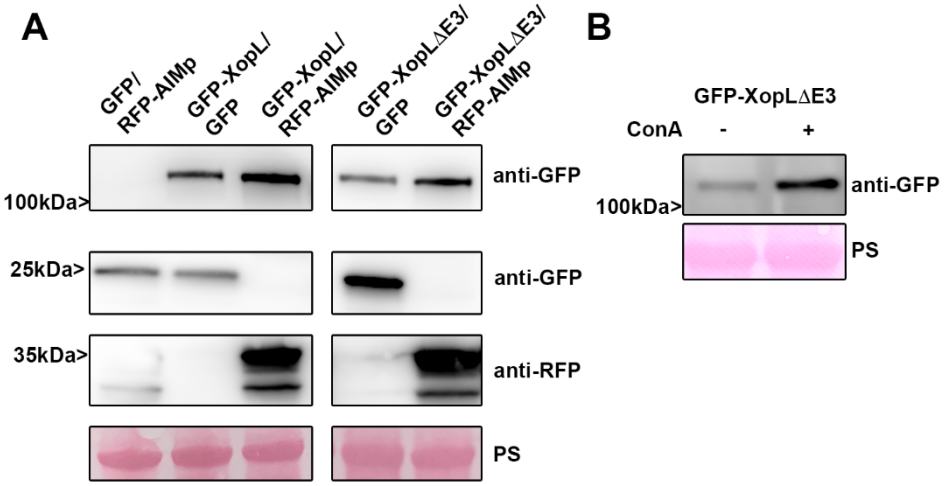


**Fig. S17: XopL ΔE3 is degraded by autophagy.**
**(A)** GFP, GFP-XopL, or GFP-XopL ΔE3 was coexpressed with RFP-AIMp or RFP control in *N. benthamiana*. Samples were taken at 2 dpi, total proteins extracted and immunoblotted using the indicated antibodies. Ponceau Staining (PS) served as a loading control.
**(B)** Immunoblot of transiently expressed GFP-XopL ΔE3 in *N. benthamiana* after treatment of ConA or DMSO carrier. Ponceau Staining (PS) served as a loading control.

**Supplemental Figure 18**

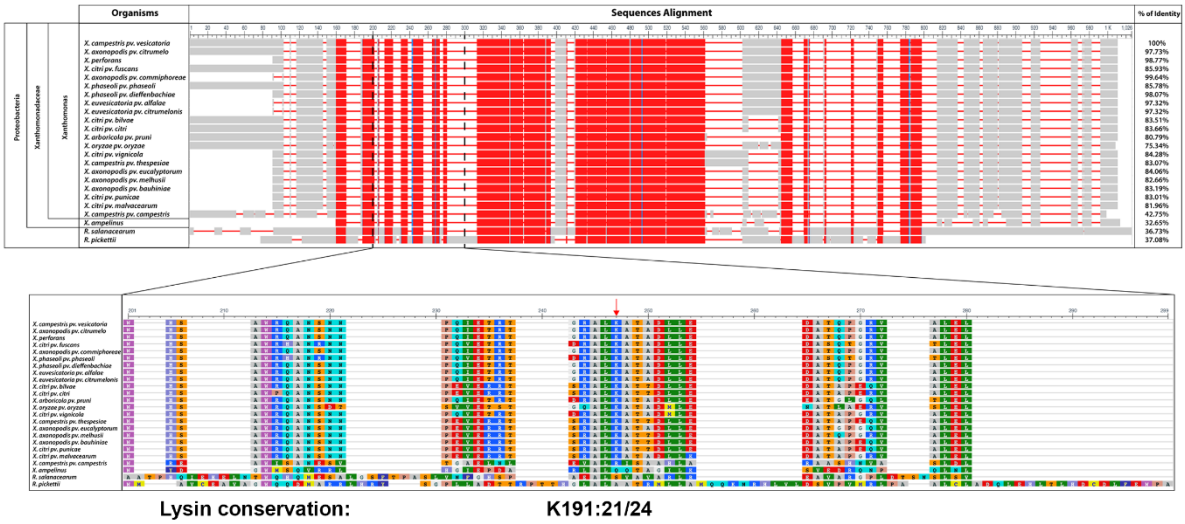


**Fig. S18: XopL K191 residue is highly conserved through the Xanthomonas genus**
**(A)** Sequence alignment of XopL protein from *Xcv* with related effectors from *Xanthomonas* genus or more distantly related plant pathogen bacteria. Colors represent amino acid conservation through the alignment, with red for highly conserved residues, blue for lower conservation and grey for no conservation. Identical amino acid percentage to XopL$^{Xcv}$ is displayed to the right of the alignment.
**(B)** Closer view of the region 201-299 of the alignment with amino acids colored according to the Rasmol coloration. Lysine K191 is indicated with a red arrow.